



WILEY

ORIGINAL ARTICLE

Effect of pore size and spacing on neovascularization of a biodegradable shape memory polymer perivascular wrap

Timothy C. Boire^{1,2} | Lauren E. Himmel³ | Fang Yu¹ | Christy M. Guth⁴ |
Bryan R. Dollinger¹ | Thomas A. Werfel^{1,5} | Daniel A. Balikov^{1,2} | Craig L. Duvall¹

¹Department of Biomedical Engineering, Vanderbilt University, Nashville, Tennessee, USA

²Department of Mechanical Engineering, Vanderbilt University, Nashville, Tennessee, USA

³Department of Pathology, Microbiology and Immunology, Vanderbilt University Medical Center, Nashville, Tennessee, USA

⁴Department of Surgery, Vanderbilt University Medical Center, Nashville, Tennessee, USA

⁵Biomedical Engineering Program, University of Mississippi, Oxford, Mississippi, USA

Correspondence

Timothy Boire, Department of Biomedical Engineering, Vanderbilt University, 2301 Vanderbilt Place, PMB 401592, Nashville, TN 37240-1592.

Email: timothy.c.boire@vanderbilt.edu

Funding information

American Heart Association, Grant/Award Number: 15PRE25610014; Foundation for the National Institutes of Health, Grant/Award Number: R01 HL122347; National Cancer Institute, Grant/Award Number: 5P30 CA68485-19; National Center for Advancing Translational Sciences, Grant/Award Number: ULI TR000445; National Science Foundation, Grant/Award Number: AIR-TT 1542996; Vanderbilt Mouse Metabolic Phenotyping Center, Grant/Award Number: U24 DK059637-16

Abstract

Neointimal hyperplasia (NH) is a main source of failures in arteriovenous fistulas and vascular grafts. Several studies have demonstrated the promise of perivascular wraps to reduce NH via promotion of adventitial neovascularization and providing mechanical support. Limited clinical success thus far may be due to inappropriate material selection (e.g., nondegradable, too stiff) and geometric design (e.g., pore size and spacing, diameter). The influence of pore size and spacing on implant neovascularization is investigated here for a new biodegradable, thermoresponsive shape memory polymer (SMP) perivascular wrap. Following an initial pilot, 21 mice were each implanted with six scaffolds: four candidate SMP macroporous designs (a–d), a nonporous SMP control (e), and microporous GORETEX (f). Mice were sacrificed after 4 ($N = 5$), 14 ($N = 8$), and 28 ($N = 8$) days. There was a statistically significant increase in neovascularization score between all macroporous groups compared to nonporous SMP ($p < .023$) and microporous GORETEX ($p < .007$) controls at Day 28. Wider-spaced, smaller-sized pore designs (223 μm -spaced, 640 μm -diameter Design c) induced the most robust angiogenic response, with greater microvessel number ($p < .0114$) and area ($p < .0055$) than nonporous SMPs and GORETEX at Day 28. This design also produced significantly greater microvessel density than nonporous SMPs ($p = 0.0028$) and a smaller-spaced, larger-sized pore (155 μm -spaced, 1,180 μm -sized Design b) design ($p = .0013$). Strong neovascularization is expected to reduce NH, motivating further investigation of this SMP wrap with controlled pore spacing and size in more advanced arteriovenous models.

KEYWORDS

neovascularization, pore spacing, pore size, shape memory polymers, hemodialysis access

1 | INTRODUCTION

Hemodialysis sustains 460,000 end-stage renal disease (ESRD) patients in the United States, and globally the number of dialysis patients is expected to more than double to 5.4 million by 2030 (System USRD, 2018; Wetmore & Collins, 2016). Arteriovenous fistulas (AVFs) and arteriovenous grafts (AVGs) are the two preferred modes of vascular access in hemodialysis, as they are far less prone to bacteremia,

No benefit of any kind will be received either directly or indirectly by the authors. A medical device startup company that has licensed this shape memory polymer wrap technology from Vanderbilt University, VenoStent, Inc., was cofounded by Dr T. C. B. after the majority of this experimental work and analysis was conducted. VenoStent, Inc. is a very early-stage, prerevenue R&D startup company years away from market. This has in no way compromised the integrity of this research.

sepsis, thrombosis, and central venous stenosis than are centralized venous catheters. However, the 2018 U.S. Renal Data System (USRDS) Annual Report indicates that 39% of AVFs placed between June 2014 and May 2016 failed to mature (i.e., primary failure), and thus were never even used for dialysis treatments (Lok et al., 2013; System USRD, 2018). Of those AVFs that do mature, 40% need interventions (i.e., 60% primary patency) and 29% are abandoned (i.e., 71% secondary patency) within 1 year (Al-Jaishi et al., 2014; Lok et al., 2013). Likewise, 19% of AVGs undergo primary failure, with primary and secondary patency rates of 30–50% and 55–70% at 1 year, respectively (Dixon et al., 2009; Huber, Carter, Carter, & Seeger, 2003; Lok et al., 2013; MacRae et al., 2016). In coronary artery bypass grafting (CABG), 10–20% of saphenous vein grafts fail within the first year, and up to 50% within 10 years (Bourassa et al., 1985; Chesebro et al., 1984; Fitzgibbon et al., 1996; Sabik, 2011; Sabik Iii, Lytle, Blackstone, Houghtaling, & Cosgrove, 2005). Similarly, 30–50% of peripheral artery bypass grafts (PABGs) fail within 5 years (Conte, 2007). AVF and AVG failures contribute to 5-year hemodialysis survival rates of just 42%, 30-day ESRD hospital readmissions of 34.2%, and a significant portion of the estimated \$2–\$3B in annual costs absorbed by the Centers for Medicare and Medicaid Services to treat these dysfunctions (System USRD, 2018).

The primary culprit of access site and vein graft failures is posited as venous stenosis caused by neointimal hyperplasia (NH), as well as lack of positive remodeling in AVF maturation failures. Surgical trauma, an order of magnitude hemodynamic increase in pressure and flow, and other factors cause vascular smooth muscle cells (VSMCs) and myofibroblasts within the vein walls to migrate toward the intima and deposit extracellular matrix proteins to form a “neointima” that obstructs blood flow through the access site and necessitates costly interventions or surgeries.

Systemic therapeutics to improve maturation and patency have so far exhibited little to marginal benefit (Alexander et al., 2005; Boire et al., 2016; Chesebro et al., 1984; Conte et al., 2006; Dixon et al., 2009; Goldman et al., 1994; Muto, Model, Ziegler, Eghbalieh, & Dardik, 2010), motivating us to prioritize therapeutic (Evans, Hocking, Kilchrist, et al., 2015; Evans, Hocking, Osgood et al., 2015) and/or device approaches localized to the vein graft, especially near the venous anastomosis where stenotic lesions typically develop (Badero, Salifu, Wasse, & Work, 2008; Cunnane, Cunnane, & Walsh, 2017; MacRae et al., 2016; Roy-Chaudhury, Sukhatme, & Cheung, 2006; Sivanesan, How, & Bakran, 1999). Perivascular approaches have focused primarily on either promoting processes involved in outward remodeling (e.g., adventitial angiogenesis or elastin fragmentation) (Hye et al., 2014) or attenuating vein wall tension and stresses with mechanical support.

Adventitial angiogenesis, an outward remodeling process by which new tissue and microvessels form on the outer, adventitial layer of vein walls, is thought to be beneficial for veins surgically connected to the arterial circulation because it can cause the outward instead of inward migration of VSMCs and myofibroblasts to mitigate NH (Angelini, Izzat, Bryan, & Newby, 1996; George et al., 2001; Jeremy et al., 2007; Mehta et al., 1998). Neovascularization (as well as accumulation of immune cells such as lymphocytes and neutrophils) induced by perivascular wraps comprised of nondegradable Dacron (Angelini et al., 1996; George et al., 2001; Jeremy et al., 2007; Mehta et al., 1998) or fast-degrading

(i.e., 1–2 month loss of strength) polyglactin (Jeremy et al., 2004; Maurus & Kaeding, 2004; Vijayan et al., 2004) may have reduced NH by serving as chemoattractants in the interstitial space between external stent and venous tissue, as well as by restoring a small blood vessel network akin to the vein's native vasa vasorum (i.e., neovasa vasorum) that may mitigate NH-inducing hypoxic conditions (Chanakira et al., 2012; McGeachie, Meagher, & Prendergast, 1989; Misra et al., 2010) and is particularly disrupted in PABG and CABG surgeries (Jeremy et al., 2007).

Unlike Dacron, polyglactin, metals, or other materials applied as an external stent, the approach tested here (“SelfWrap”) is a slowly biodegradable, poly(ϵ -caprolactone) (PCL)-based shape memory polymer (SMP) wrap with artery-mimetic mechanical stiffness that is moldable at body temperature. Because these SMPs melt below body temperature, transitioning from an elastic to a viscoelastic, more gelatinous state (Boire et al., 2015), SelfWrap is designed to mold to the patient's specific geometry at the venous anastomosis. This better surface area coverage around the anastomosis is hypothesized to promote more substantial and uniform outward vein remodeling, and better dissipate heightened wall tension and stresses in the AV environment. The viscoelastic property of the material is tuned to be artery-mimetic in order to reduce compliance mismatch issues that can result in NH (Abbott, Megerman, Hasson, L'Italien, & Warnock, 1987; Ballyk, Walsh, Butany, & Ojha, 1997; Haruguchi & Teraoka, 2003; Li, Terry, Shiu, & Cheung, 2008; Okuhn et al., 1989; Stewart & Lyman, 1992; Trubel et al., 1995). The slow degradability of SelfWrap, estimated at 1–2 years *in vivo*, better ensures sufficient mechanical support beyond the critical vein remodeling period of at least 3 months, while also mitigating risk of infection, chronic inflammation, and NH-inducing compliance mismatches that can beset nondegradable implants (Abbott et al., 1987; Ballyk et al., 1997; Boire et al., 2016; Bunt, 2001; Edwards, Martin, Jenkins, & Mulherin, 1987; Jeremy et al., 2004; Okuhn et al., 1989; Trubel et al., 1995; Vijayan et al., 2004). The SMP material utilized is intended to overcome shortcomings related to previous material selection (e.g., nondegradable, too stiff), and herein we study the important parameter of material porosity.

Parameters such as pore size and spacing have been shown to influence angiogenic responses induced by synthetic and natural polymeric implants. Pore parameters affect the surface area-to-volume ratio and topology of implants, which plays a role in the type and extent of inflammatory reaction and outcomes such as neovascularization (Lake et al., 2015; Zhang, Wang, Liu, & Kodama, 2004; Zhu, Schuster, & Klinge, 2015). However, few studies have directly examined the effect of external stent pore size, or other pore parameters, on neoadventitial growth and NH. In general, larger pores exhibit less scarring, inflammatory infiltrate, and connective tissue, but pore size requirements will differ depending on the biomaterial selected (Greca et al., 2008; Klosterhalfen & Klinge, 2013; Zhu et al., 2015). For example, polypropylene requires pores larger than 1 mm while pores smaller than 650 μm are adequate for PVDF to obviate scarring between pores in abdominal wall hernias (Klinge & Klosterhalfen, 2012). To enhance bone tissue formation by vascularization, pore sizes greater than 300 μm are recommended (Karageorgiou & Kaplan, 2005; Roosa, Kemppainen, Moffitt, Krebsbach, & Hollister, 2010). While there is a relative dearth of experimental data available, it is hypothesized based on the current literature that pore sizes should be >300 μm with spacings >100 μm (but not too

far beyond the 100–200 μm diffusion limit for oxygen to avoid hypoxia) (Carmeliet & Jain, 2000) for polymeric external stents. Toward testing in more advanced AVF/AVG models, this study seeks to define pore sizes and spacings of an SMP mesh that maximize neovascularization in a subcutaneous murine model.

2 | METHODS

2.1 | Fabrication of crosslinked SMP meshes

PCL-based SMPs were synthesized and UV-crosslinked in a manner similar to our previously reported procedure (Boire et al., 2015), then were laser-ablated to induce pores; see Appendix for more details.

2.2 | Pore characterization

Porosity was calculated from pore size and spacing measurements of scanning electron microscopy (SEM) images of scaffolds (see Appendix).

2.3 | Mechanical characterization

Moduli at 37°C, E_{tn} (37°C) were determined (Abbott et al., 1987; Deeken et al., 2011); see Appendix.

2.4 | Cytotoxicity testing

See Appendix.

2.5 | Animal model

Similar to that described by Kucharíková, Vande Velde, Himmelreich, and van Dijck (2015); see Appendix.

2.6 | SEM of scaffold–tissue interfaces

See Appendix.

2.7 | Histological analysis

See Appendix for details. Histological analysis was performed by a board-certified veterinary pathologist masked to experimental conditions. Each sample was assigned semi-quantitative scores to assess the degree of neovascularization, inflammation, and fibrogenesis utilizing a scoring criterion adapted from Lake et al. and Deeken et al. (Table 1, Figure 1) (Deeken et al., 2011; Lake et al., 2015). Cumulative scores were calculated by summing the scores of each of these three categories.

2.8 | Immunohistochemistry

See Appendix, which contains a list of primary antibodies (Table S1), CD31 microvessel detection of capillaries (and small arterioles) in the approximate range of 3.4–28 μm inner diameter (Pappano & Gil Wier, 2013) (Table S2), and macrophage phenotype characterization algorithm details (Figure S1, Tables S3–S5) (Bankhead et al., 2017) and calculations (Brown et al., 2012).

2.9 | Proteomics analysis

Comparisons of relative peptide and protein amounts were performed using MaxQuant-LFQ software (Cox et al., 2014); see Appendix for details of sample prep, LC–MS/MS, and analysis.

2.10 | Statistical analysis

See Appendix.

TABLE 1 Histological scoring criterion

Score	0	1	2	3
Neovascularization	No blood vessels present	Vessels only at periphery	Vessels present within interstices but not bridging	Vessels bridge implant in at least one focus
Fibrogenesis	Connective tissue bridges implant in multiple foci	Connective tissue bridges implant focally	Fibrosis at periphery beginning to invest interstices	Peripheral fibrosis only
Inflammation	Marked: Inflammation consists of a thick, circumferential cuff of neutrophils, multinucleated giant cells, histiocytes, lymphocytes, and plasma cells	Moderate: Inflammation consists of moderate, multifocal/segmented aggregation of multinucleated giant cells, histiocytes, lymphocytes, and plasma cells with fewer neutrophils	Mild: Inflammation consists of mild, multifocal/segmental aggregates of multinucleated giant cells, histiocytes, lymphocytes, and plasma cells with fewer neutrophils; >50% of implant's circumference is affected	Minimal: Inflammation consists of mild, multifocal aggregates of multinucleated giant cells, histiocytes, lymphocytes, and plasma cells with infrequent neutrophils; <50% of implant's circumference is affected.

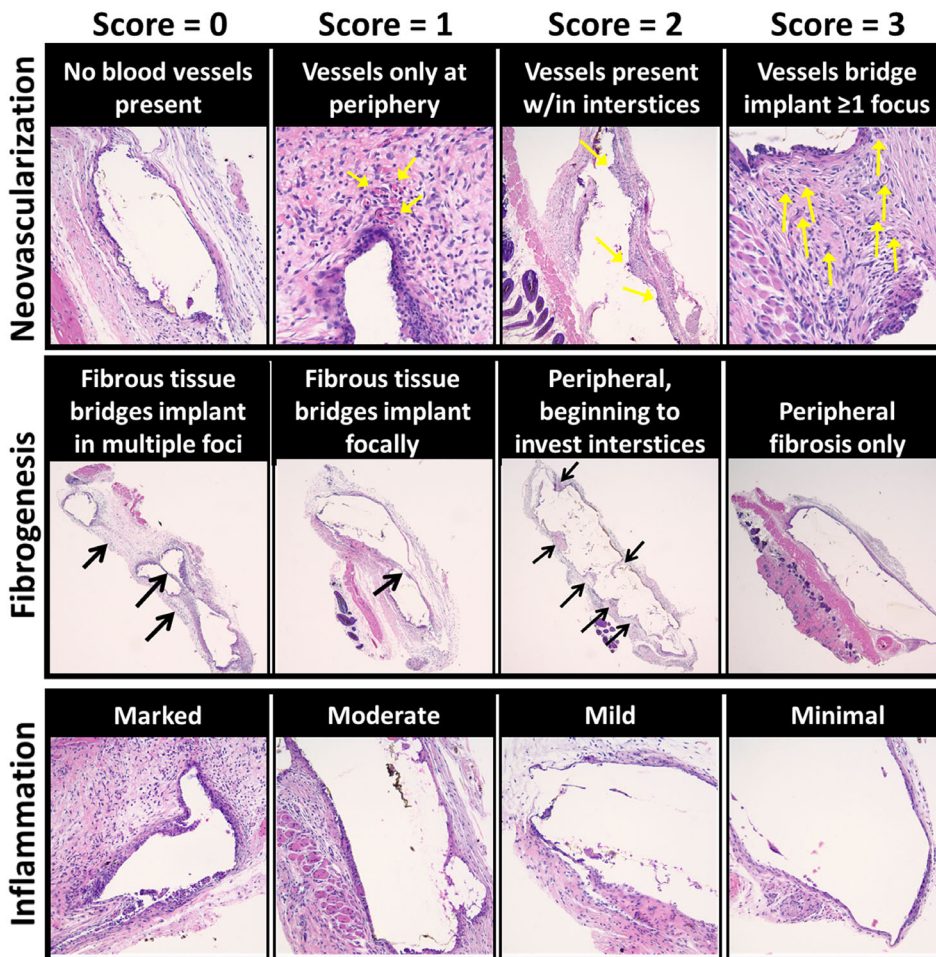


FIGURE 1 Illustration of histological scoring. Representative H&E-stained histological sections of the polymer–tissue interface illustrate tissue responses that correspond to a given score from 0 to 3 according to the masked pathologist. (Top) From left to right, sections depict a low to a high amount of neovascularization (yellow arrows) at original magnifications of $\times 200$, $\times 400$, $\times 100$, and $\times 400$, respectively. (Middle) From left to right, fibrogenesis is less apparent, with arrows indicating bridging (original magnification $\times 40$). (Bottom) From left to right, inflammation is milder and less marked (original magnification $\times 200$)

3 | RESULTS

As an initial investigation into the influence of pore size and spacing on tissue responses from SelfWrap designs, a 14-day pilot study was first conducted in which six SMP scaffolds (Figure S2, Table S6) of varying pore size and spacing were implanted in the dorsal subcutaneous pocket of C57BL/6J male mice in accordance with Vanderbilt's IACUC ($N = 3\text{--}4$ per scaffold type). A grouped analysis of the three different pore sizes ($1 = 293 \pm 41 \mu\text{m}$, $2 = 665 \mu\text{m} \pm 24 \mu\text{m}$, $3 = 1,067 \pm 35 \mu\text{m}$) and two different pore spacings ($a = 172 \pm 55 \mu\text{m}$, $b = 224 \pm 56 \mu\text{m}$) revealed a significantly higher cumulative score for the wider-, $220 \mu\text{m}$ -spaced designs than the narrower-, $170 \mu\text{m}$ -spaced designs via a two-tailed Mann–Whitney U test ($p = .0099$, Figure S3). Moreover, a two-way analysis of variance (ANOVA) of a linear regression of cumulative scores ($R^2 = .523$, $p = .0012$ for spacing) followed by a two-tailed Tukey's post hoc test identified that Design 2b ($230 \mu\text{m}$ -spaced, $665 \mu\text{m}$ -sized) had a significantly higher cumulative score than its narrower-, $152 \mu\text{m}$ -spaced counterpart, Design 2a ($p = .0332$). This implied that the wider-spaced ($\sim 220 \mu\text{m}$) designs elicited more favorable tissue responses than smaller-spaced ($\sim 170 \mu\text{m}$) ones through some combination of more neovascularization and/or less inflammation and fibrosis.

Based on this observation, we sought to determine whether an optimal SelfWrap design with significantly higher neovascularization score, and potentially less inflammation and fibrogenesis, could be identified from a more highly powered longitudinal study (power analysis in Appendix, Figure S4). Macroporous SMP Scaffold Designs a–d were fabricated that possessed similar pore sizes and spacings to Designs 2a, 3a, 2b, and 3b in the pilot study, respectively. Designs a–d possessed two statistically unique pore spacings ($a, b = 151 \pm 50 \mu\text{m}$ and $c, d = 229 \pm 51 \mu\text{m}$) and pore sizes ($a, c = 635 \pm 51 \mu\text{m}$ and $b, d = 1,160 \pm 64 \mu\text{m}$) to enable independent evaluation of pore spacing and size effects on material properties and in vivo responses (statistical analysis of pore size and spacing described in Appendix, Table S7). Other designs served as nonporous or microporous controls: non laser-ablated PCL-based SMPs (Design e) and a $\sim 6 \times 8 \times 0.64 \text{ mm}^3$ piece of commercially available Standard Wall GORETEX tubing comprised of ePTFE with $10\text{--}30 \mu\text{m}$ -sized micropores (Design f) (Table 2, Figure 2) (Kim, Lim, Park, & Lee, 2014).

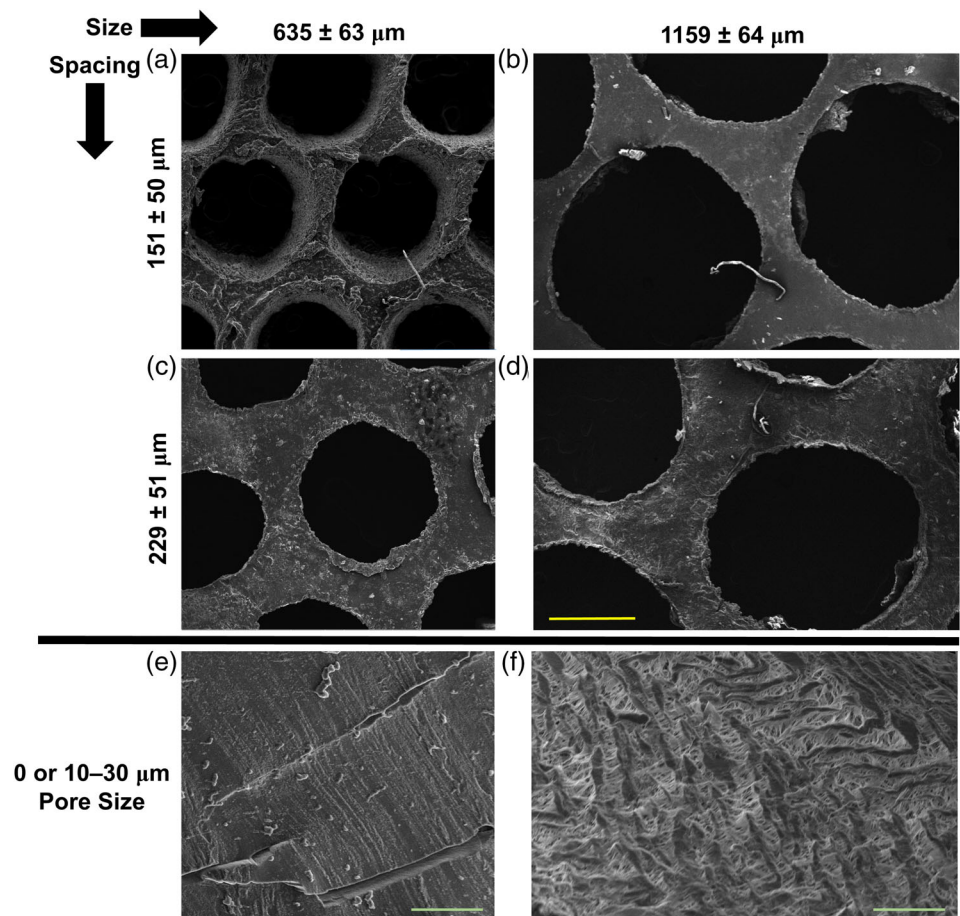
Prior to implantation, mechanical properties were evaluated for SMP Designs a–e. Young's modulus at body temperature (E_{tn} (37°C), maximum stress (σ_{max}), and maximum strain (ϵ_{max}) were measured isothermally at 37°C . Young's moduli of both nonporous (2.4 ± 0.86) and porous (mean = $0.57\text{--}1.11 \text{ MPa}$) SMP designs were very close to the average physiological modulus of healthy human coronary arteries

TABLE 2 Pore properties for statistically powered mouse cohort

Design	Polymer	Pore diameter (μm)	Spacing (μm)	Estimated void area ($\text{mm}^2 \times 10^3$)	Estimated porosity (%)	E_{tn} (37°C) (MPa)	ϵ_{max} (%)	σ_{max} (MPa)
A	SMP	627 \pm 50	148 \pm 45	\sim 620	\sim 59	0.92 \pm 0.26	60.0 \pm 13	0.15 \pm 0.03
B	SMP	1,180 \pm 78	155 \pm 52	\sim 2,200	\sim 71	0.57 \pm 0.25	106 \pm 17	0.17 \pm 0.02
C	SMP	640 \pm 71	223 \pm 42	\sim 640	\sim 50	1.08 \pm 0.50	78 \pm 65	0.26 \pm 0.06
D	SMP	1,140 \pm 86	226 \pm 58	\sim 2,000	\sim 62	1.11 \pm 0.12	76 \pm 46	0.29 \pm 0.08
E	SMP	Non/micro	N/A	N/A	N/A	2.4 \pm 0.86	52 \pm 30	0.44 \pm 0.09
F	GORETEX (ePTFE)	10–30 μm (Kim, Lim, Park, & Lee, 2014)	N/A	N/A	N/A	15.5 \pm 1.6 (Kim, Lim, Park, & Lee, 2014)	139 \pm 11 (Kim, Lim, Park, & Lee, 2014)	24.3 \pm 1.8 (Kim, Lim, Park, & Lee, 2014)
150	SMP	635, 1,160	151 \pm 50	\sim 620, 2,200	\sim 59, 71	0.9, 0.57	60, 110	0.16
230	SMP	635, 1,160	229 \pm 51	\sim 640, 2,000	\sim 50, 62	1.1	78, 72	0.26
640	SMP	635 \pm 63	151, 229	\sim 630	\sim 59, 50	0.92, 1.1	60, 78	0.15, 0.26
1,160	SMP	1,160 \pm 64	151, 229	\sim 2,100	\sim 71, 62	0.57, 1.1	110, 72	0.17, 0.26
0–30	SMP, ePTFE	0–30	N/A	N/A	N/A	2.4, 15.5	52, 139	0.44, 24.3

Abbreviation: SMP, shape memory polymer.

FIGURE 2 Pore designs for statistically powered mouse cohort. Scanning electron microscopy (SEM) micrographs of the six scaffolds used as implants in the larger mouse cohort evaluating neovascularization, inflammation, and fibrogenesis over the course of 28 days. Macroporous Designs –(a–d) are paired by equivalent size and spacing to evaluate the influence of these parameters on in vivo responses. Images are scaled to the same magnification for –(a–d) (top yellow scale bar = 500 μm), while nonporous shape memory polymer (SMP) (Design e) and microporous ePTFE (Design f) implants are shown at $\times 10$ of this magnification (bottom green scale bars = 50 μm)



(1.48 MPa) (Karimi, Navidbakhsh, Shojaei, & Faghihi, 2013), suggesting suitability for vascular and soft tissue applications from a mechanical perspective. As expected, ablating pores in the crosslinked polymer designs resulted in significant decreases in E_{tn} (37°C) and σ_{max} for all of the designs ($p < .003$). Decreasing the spacing of the pores from

229 \pm 51 μm (c,d) to 151 \pm 51 μm (a,b) further reduced both E_{tn} (37°C) and σ_{max} , but not in a statistically significant manner when evaluated as part of the five-group cohort. However, pairwise comparisons of pore spacing and size revealed a statistically significant decrease in σ_{ma} when spacing is reduced from 230 to 150 μm

($p = .0025$), but not when pore size is changed approximately twofold ($p = .3662$). These results suggest that mechanical properties are more dependent on pore spacing than pore size.

An initial *in vitro* cytotoxicity test was also conducted on the SMP material prior to implantation (Appendix). Human dermal fibroblasts cultured with media leached from SMP and PCL scaffolds or coincubated with these polymer samples resulted in >80% viability over 4 days relative to TCPS (Figure S5). This result, along with the 14-day mouse pilot study data and artery-mimetic tensile stiffness of these SMP scaffolds, motivated additional *in vivo* experimentation.

3.1 | SEM characterization of the polymer–tissue interface

To evaluate the effect of pore size and spacing on neovascularization, inflammation, and fibrosis, 21 mice were subcutaneously implanted with the 6 different scaffolds (Figure 2) through 6 independent

incisions to keep their placement separated on the mouse dorsum. Responses of tissue explants from each design were characterized through SEM microscopy on Days 4, 14, and 28. The SEM micrographs provide a three-dimensional visualization of certain architectural features of the polymer–tissue interfaces, such as deposition of sheets of extracellular matrix components, connective tissue, and cellular milieu on and surrounding scaffold surfaces, including within pores (Figure 3). On Day 4, the polymer is still mostly separated from the native tissue in all designs, with visible clefts apparent (blue arrows). Inflammatory cells begin to infiltrate the macropores as early as Day 4. As the inflammatory response from the SMP material progressed to Day 14, connective fibrovascular tissue was observed penetrating the pores. Although SEM micrographs on Days 4 (Figure S6), 14 (Figure S7), and 28 (Figure S8) do not allow for evaluation of margins of all of the designs, it appears that the tissue–implant interface begins to blur together multifocally in porous designs by Day 14. This is less apparent in nonporous ones, where clefts are still apparent (Figure 3). In general, the polymer appeared to be more integrated into

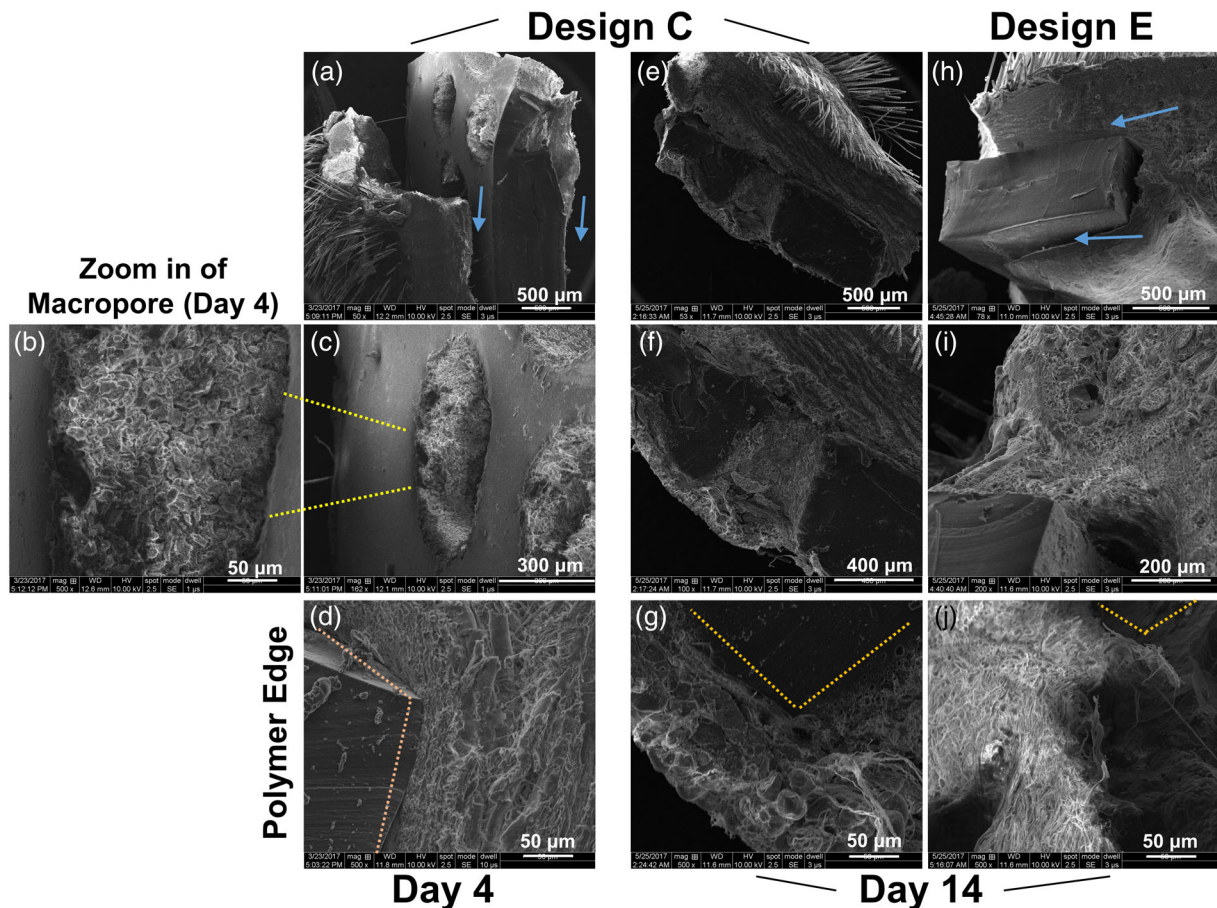


FIGURE 3 Scanning electron microscopy (SEM) micrographs of polymer–tissue interface. (a–d) On Day 4, the material is mostly separated from the native tissue in all designs, including Design (c) here, with visible clefts apparent (blue arrows in (a)). (b,c) Inflammatory cells begin to infiltrate the macropores as early as Day 4. (d) Further zooming in to the polymer edge (dashed orange line), there appears to be some clear separation between polymer and tissue. (e–g) As the inflammatory response from the shape memory polymer (SMP) material progresses to Day 14 for macroporous designs such as Design (c) here, (e,f) connective fibrovascular tissue begins to penetrate the pores and (g) the polymer is more integrated into the host tissue. (h) In contrast, nonporous Design (e) still has some apparent clefts between the polymer and tissue on Day 14 (blue arrows in (h)). (i,j) Diverse cell and tissue architectures, such as sheets of extracellular matrix components, are visible in all implants, including Design (e) on Day 14 here

the host on Day 28, with thicker, more established fibrovascular tissue engulfing the polymer (Figure S8).

3.2 | Histological scoring of the polymer–tissue interface

These observations over time were consistent with histological scoring results for Designs a–f (Figure 4, Table S8, Figure S9) using the described histological scoring protocol (Table 1, Figure 1). Namely, both neovascularization and fibrogenesis increased significantly over time for

macroporous designs, but this trend was less obvious for the controls. On Day 4, histological analysis of H&E staining revealed that there was very little fibrosis (fibrogenesis score = 3) or neovascularization (neovascularization score = 0) detected for any of the samples, while inflammation was mostly mild (>2)—some multifocal aggregates of multinucleated giant cells, histiocytes (e.g., macrophages), lymphocytes, and plasma cells were present, but without abundance of neutrophils.

On Day 14, there was an increase in neovessels and connective tissue present, although this was primarily restricted to the periphery of the polymer–tissue interface; neovascularization scores were >1 for all designs except for nonporous SMP Design e (0.88 ± 0.36), and

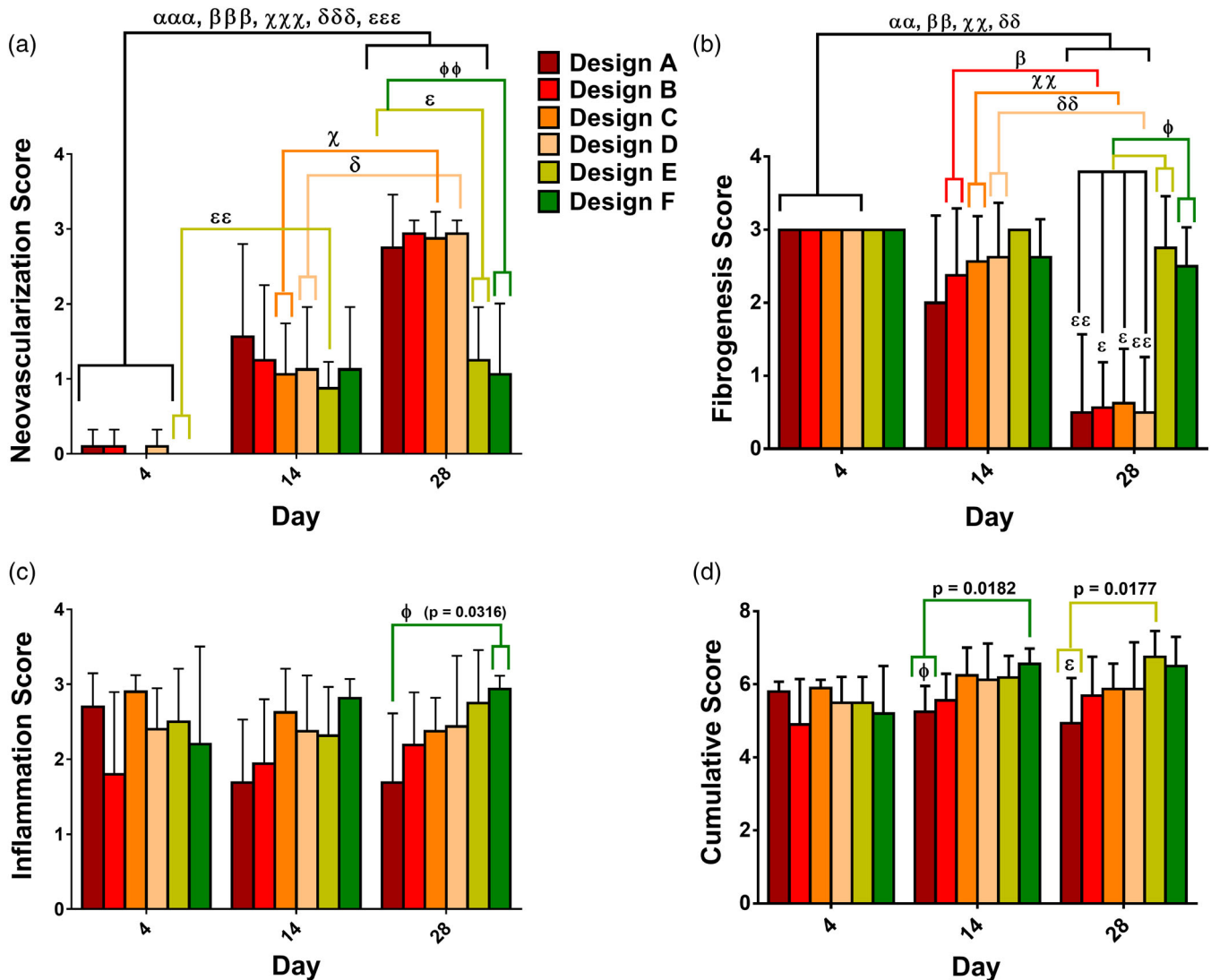


FIGURE 4 Histological scores from subcutaneous murine implantation. Comparisons of (a) neovascularization, (b) fibrogenesis, (c) inflammation, and (d) cumulative score semiquantitative assessments for Designs (a–f). Macroporous Designs (a–d) exhibit significantly more neovascularization and fibrogenesis than the nonporous shape memory polymer (SMP) (Design (d)) and microporous ePTFE (Design (e)) controls over 28 days. Inflammation was mild for most designs, but more moderate and intensified in the smaller-spaced, smaller-sized (148 μm -spaced, 627 μm -sized) Design (a), which translated to a lower clinical score. Greek symbols correspond to statistically significant differences detected by Kruskal–Wallis analysis of variance (ANOVA) and post hoc Tukey's between test group and the group with the same name in the English alphabet: $\alpha = p < .05$ between Design (a) and test, $\beta = p < .05$ from Design (b), $\gamma =$ diff. from (c), $\delta =$ diff. from (d), $\varepsilon =$ diff. from (e), $\theta =$ diff. from (f). * = <.05, ** = .005, *** = <.0005. The color of each line indicating a significant difference matches that of the respective design, unless the line represents multiple groups, in which case it is black

fibrogenesis scores were >2 for all designs. Applying a Kruskal–Wallis and Dunn's post hoc comparison of all combined designs at the three different time points indicated a significant increase in neovascularization from Days 4 to 14 ($p < .0001$) but no differences in fibrogenesis from Days 4 to 14. Inflammation was moderate for closer-spaced Designs a and b, with inflammation scores <2 reflective of more multifocal aggregation of inflammatory cells (e.g., multinucleated giant cells, histiocytes, etc.) and $>50\%$ of the implant's circumference affected; in contrast, inflammation remained mild for the other designs (inflammation score >2). There was a statistically significant increase in neovascularization score from Days 4 to 14 for Design e ($p = .0082$) and a lower cumulative score from Design a than Design f on Day 14 ($p = .0177$). Pairing the cohort into groups of equivalent pore spacing ($150\ \mu\text{m}$ [a,b] vs. $230\ \mu\text{m}$ [c,d] vs. non/microporous [e,f]) revealed that the inflammation and cumulative scores were significantly lower for the $150\ \mu\text{m}$ -spaced group ($p < .037$) and no different between the $230\ \mu\text{m}$ -spaced and non/microporous group ($p > .999$). Pairing by equivalent pore sizes ($640\ \mu\text{m}$ [a,c] vs. $1,160\ \mu\text{m}$ [b,d] vs. $0\text{--}30\ \mu\text{m}$ [e,f]), on the other hand, revealed no significant differences between groups. These results therefore suggest that there is more intense inflammation with closer-spaced pore Designs a and b at 14 days, and pore size does not influence the overall inflammatory reaction at this point.

Neovascularization and fibrogenesis continued to progress in the macroporous designs from Days 14 to 28, with vessels bridging implants in at least one focus (median neovascularization score of 3 for Designs a–d) and connective tissue bridging at multiple foci (median fibrogenesis score of 0 or 0.5 for a–d) for most of the porous samples. The increase in connective tissue bridging can be visualized by both H&E (Figure 5) and Masson's trichrome staining on the designs at the three different timepoints (Figure S10). Non/microporous controls e

and f were the opposite, with minimal neovascularization (neovascularization score = 1.16 ± 0.81) and fibrogenesis (fibrogenesis score = 2.63 ± 0.62). All porous and non/microporous designs were statistically significant from each other by neovascularization and fibrogenesis scores. Inflammation remained mild (inflammation score = 2) to minimal (inflammation score = 3) for all designs except for a, which was more moderate (1.69 ± 0.92). As such, Design a had a significantly lower inflammation score ($p = .0318$) and cumulative score ($p = .0182$) than Design f. Pairwise pore spacing and size comparisons revealed significant lower inflammation and cumulative scores for the small spacing ($p \leq .001$) and small pore size groups ($p \leq .0029$) compared to non/microporous controls. These results suggest that a small pore spacing and size combination (Design a) may elicit a more intense, moderate inflammatory response at 28 days.

3.3 | CD31 quantification

To further assess and compare neovascularization responses of designs, a microvessel detection algorithm was run that quantified the total number of vessels (TNV), total and average vessel area, average vessel perimeter, and microvessel density by detecting the DAB that was counterstained against CD31 (Figure 6). TNV, total vessel area, and microvessel density were weighted to total tissue area and normalized to Day 4 (see Appendix). As the objective was to detect new, scaffold-induced vascular ingrowth, or capillary formation, as a model of perivascular engraftment (rather than create a conduit to supply blood flow to ischemic tissue), large, preexisting vessels $>28\ \mu\text{m}$ were intentionally excluded from this analysis. Consistent with neovascularization score trends over time, there was a significant

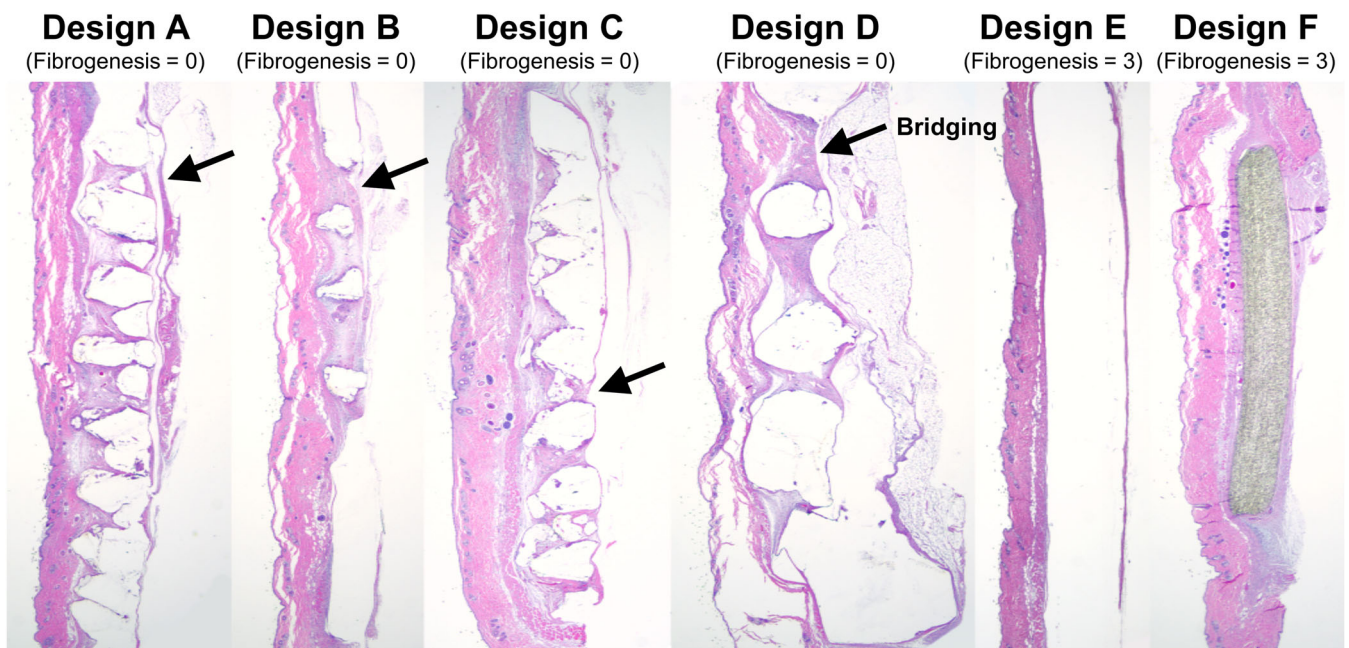


FIGURE 5 View of bridging of connective tissue. In H&E-stained sections, it appears that smaller pore Designs (a) and (c) undergo thinner bands of bridging than larger pore Sizes (b) and (d). Arrows indicate sites of bridging. Original magnification = $\times 20$

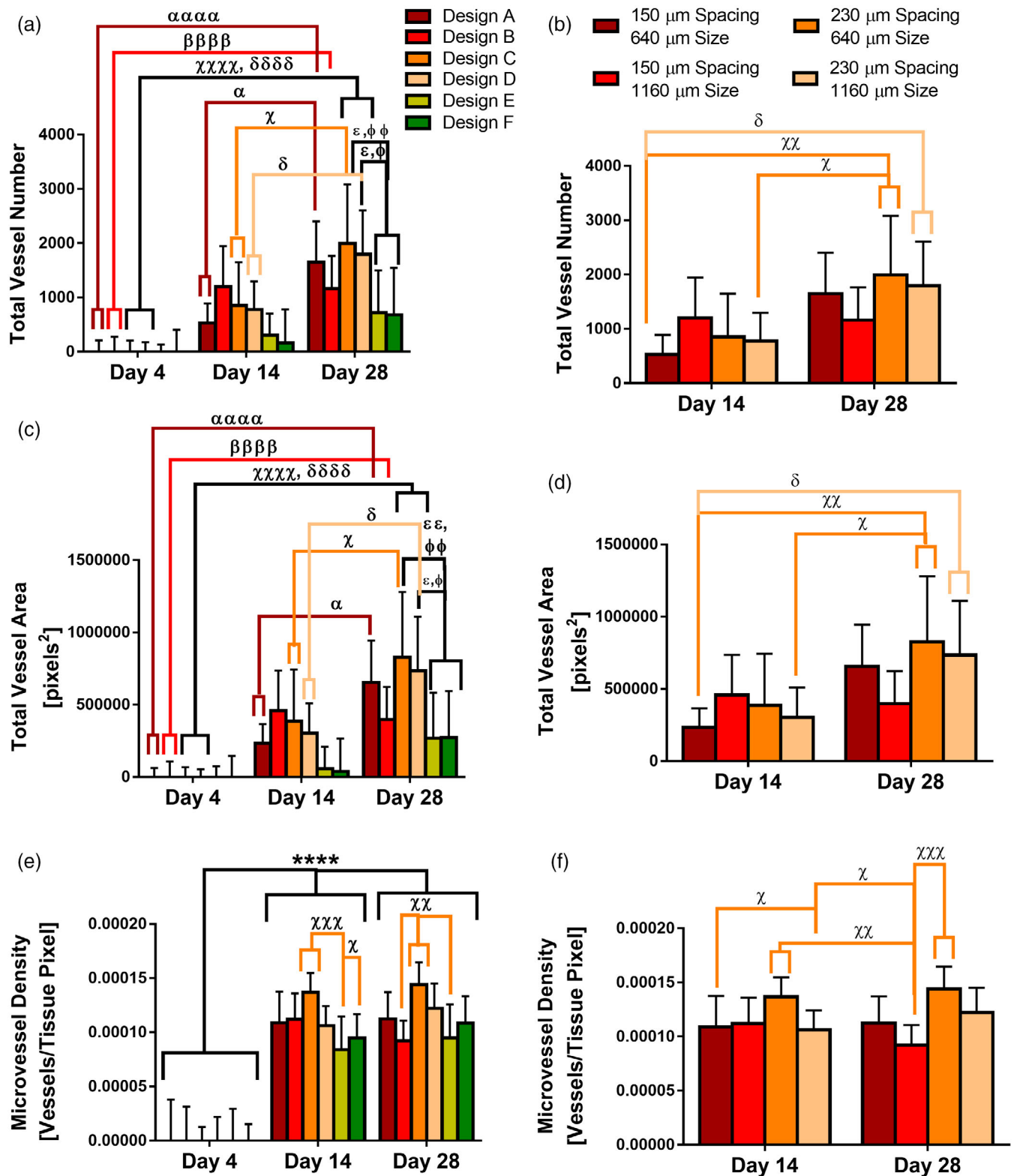


FIGURE 6 Quantification of neovascularization from anti-CD31 DAB Detection Algorithm. Total vessel number, total vessel area, and microvessel density weighted to total tissue area for each sample were normalized to Day 4 data in order to match the observation that Neovascularization scores were essentially zero at that time point, which helps to minimize false positives. Aside from significant increases over time for some of the porous designs, there were significant differences detected between the wider-spaced, smaller pore Design (c) and non/microporous controls (as well as Design (b) for microvessel density) for all three of these neovascularization parameters at Day 28. Design (d) ranked second for all of these parameters. Greek symbols correspond to statistically significant differences detected by either two-way (top) or three-way (bottom) analysis of variance (ANOVA) and post hoc Tukey's test. Symbols: $\alpha = p < .05$ between Design (a) and test, $\beta = p < .05$ from Design (b), $\gamma =$ diff. from (c), $\delta =$ diff. from (d), $\epsilon =$ diff. from E, $\theta =$ diff. from (f). * = $<.05$, ** = $.005$, *** = $<.0005$. The color of each line indicating a significant difference matches that of the respective design, unless the line represents multiple groups, in which case it is black. 1 pixel = 0.5 μm

increase in the normalized TNV, total vessel area, and microvessel density from Days 4 to 28 for all designs. Designs a, c, and d also exhibited a significant increase in TNV and total vessel area from 14 to 28 days, while there were no significant increases from Days 14 to 28 in terms of microvessel density. No significant trends or differences were detected for average vessel area, perimeter, or lumen diameter (Figure S11). The average 28-day lumen diameter across all groups was approximately $7.9 \pm 0.85 \mu\text{m}$, consistent with a typical capillary size of 5–10 μm (Pappano & Gil Wier, 2013).

Wider-spaced Designs c and d demonstrated significantly higher TNV and total vessel area than non/microporous controls on Day 28, and ranked highest and second highest, respectively, in terms of TNV, total vessel area, and microvessel density. Grouping by pore spacing and size, all macroporous groups had significantly greater TNV and total vessel area at Day 28 than non/microporous controls ($p < .0058$). Only the 230 μm -spaced ($p < .0002$) and 640 μm -sized groups ($p < .0001$) increased significantly over time from Days 14 to 28 in terms of TNV and total vessel area ($p < .0001$).

Microvessels were significantly denser on Day 14 for the 640 μm -sized, 230 μm -spaced Design c than non/microporous controls e ($p = .0009$) and f ($p = .0149$). On Day 28, Design c had greater microvessel density than both nonporous Design e ($p = .0024$) and the 1,140 μm -sized, 150 μm -spaced Design b ($p = .0013$), and had a strong trend relative to Design f ($p = .0634$). Pairwise pore spacing and size comparisons indicated that the 230 μm -spaced design group exhibited significantly higher microvessel density on Day 28 than both the 150 μm -spaced ($p = .0015$) and non/microporous groups ($p = .0012$), while the 150 μm -spaced group had significantly denser microvessels than control on Day 14 only ($p < .0399$). Both the 640 ($p = .0074$) and 1,160 ($p = .0420$) μm -sized group designs were denser than control at Day 28.

A three-way ANOVA assessing the influences of time, pore size, and pore spacing for macroporous designs on Days 14 and 28 implied that the wider spaced, smaller pore Design c was greatest in microvessel density, whereas time was the most important variable for total microvessel number and area. Pore spacing ($p = .0004$) and size ($p = .0029$) were the only variables identified to have a significant impact on microvessel density. The 28-day microvessel density from Design c was significantly greater than Design b (150 μm /1160 μm) at 28 days ($p = .0005$) as well as Designs a and d at 14 days ($p = .0481$ and $.0256$, respectively). Density of Design c at 14 days was also significantly higher than Design b at 28 days ($p = .0046$). These results suggest that the wider-spaced, smaller pore design (Design c) was most conducive to microvessel formation.

3.4 | Macrophage phenotype characterization

A pan macrophage marker (F4/80), M1 macrophage marker (iNOS), and M2 macrophage marker (CD206) were utilized to further characterize the inflammatory reaction within the polymer–tissue interface. It was expected that more favorable and less marked inflammatory responses would exhibit more of a switch to an M2 macrophage

phenotype over time. It was also anticipated that transient upregulation of an M1 macrophage phenotype would correlate with an increase in neovascularization (Yang et al., 2016), and that the relatively inert (Koehler et al., 2003), microporous ePTFE control (Design f) would have lower F4/80 and iNOS positivity than macroporous SMP Designs a–d. On Days 14 and 28, Design f had the lowest positivity for F4/80 (0.583 ± 0.091 and 0.546 ± 0.15 , respectively) and was distinct from all other designs in this regard ($p < .0001$), which implied less macrophages present from GORETEX implantation as expected (Figure 7). Design f was also the only design that decreased in F4/80 positivity over time ($p = .0060$ from Days 4 to 28). The iNOS positivity was also significantly lower for Design f than Designs a, b, and c on Day 28 ($p < .0052$). On Day 28, Design f exhibited a significantly higher CD206/iNOS ratio than all other designs ($p < .0353$), suggesting the wound has been more fully resolved with the ePTFE microporous control, whereas inflammation-mediated neovascularization and fibrogenic processes may still be ongoing without full wound resolution in the other designs.

The most pro-angiogenic design identified from the CD31 detection results, Design c, appeared to transiently upregulate an M1 macrophage phenotype, as evidenced by the iNOS positivity results. The iNOS positivity was significantly higher in Design c than Design a on Day 4 ($p = .0192$), and iNOS positivity decreased significantly from Days 4 to 14 for Designs c and b ($p < .0091$). Design c also decreased significantly in iNOS positivity from Days 4 to 28 ($p = .0202$), as did Design f ($p = .0219$). Designs d and f decreased significantly in iNOS positivity from Days 14 to 28 ($p < .0246$). On Day 28, Design d had significantly lower iNOS positivity than the closer-spaced Design b ($p = .0033$), as did Design e ($p = .0381$), which implied that the wider-spaced design (d) may better promote wound healing resolution (Yang et al., 2016).

Combining immunohistochemistry (IHC) staining data of groups based on equivalent pore size and spacing revealed interesting insights with regard to macrophage phenotype. On Day 14, smaller pores (a + c, 635 μm diameter) exhibited significantly greater CD206 positivity (mean difference = 0.0452 , $p = .0141$), lower iNOS positivity (mean difference = -0.0655 , $p = .0017$), and a higher CD206/iNOS ratio (mean difference = 0.463 , $p = .0004$) than larger pores (b + d, 1160 μm diameter). On Day 28, smaller pores again were more positive for CD206 (mean difference = 0.0322 , $p = .0147$), while larger spacings (c + d, 230 μm) had significantly lower iNOS positivity (mean difference = 0.0687 , $p = .0304$). No differences were detected for F4/80 positivity. Taken together, this implies that the ~230 μm -spaced, 640 μm -sized group (Design c, the most pro-angiogenic one) elicits an inflammatory response characterized by more of the “tissue remodeling” M2 phenotype than the other macroporous designs.

3.5 | Proteomics analysis

In order to elucidate possible molecular explanations for the increased neovascularization observed with SMP macroporous implants, protein digests extracted from the polymer–tissue interface of each design

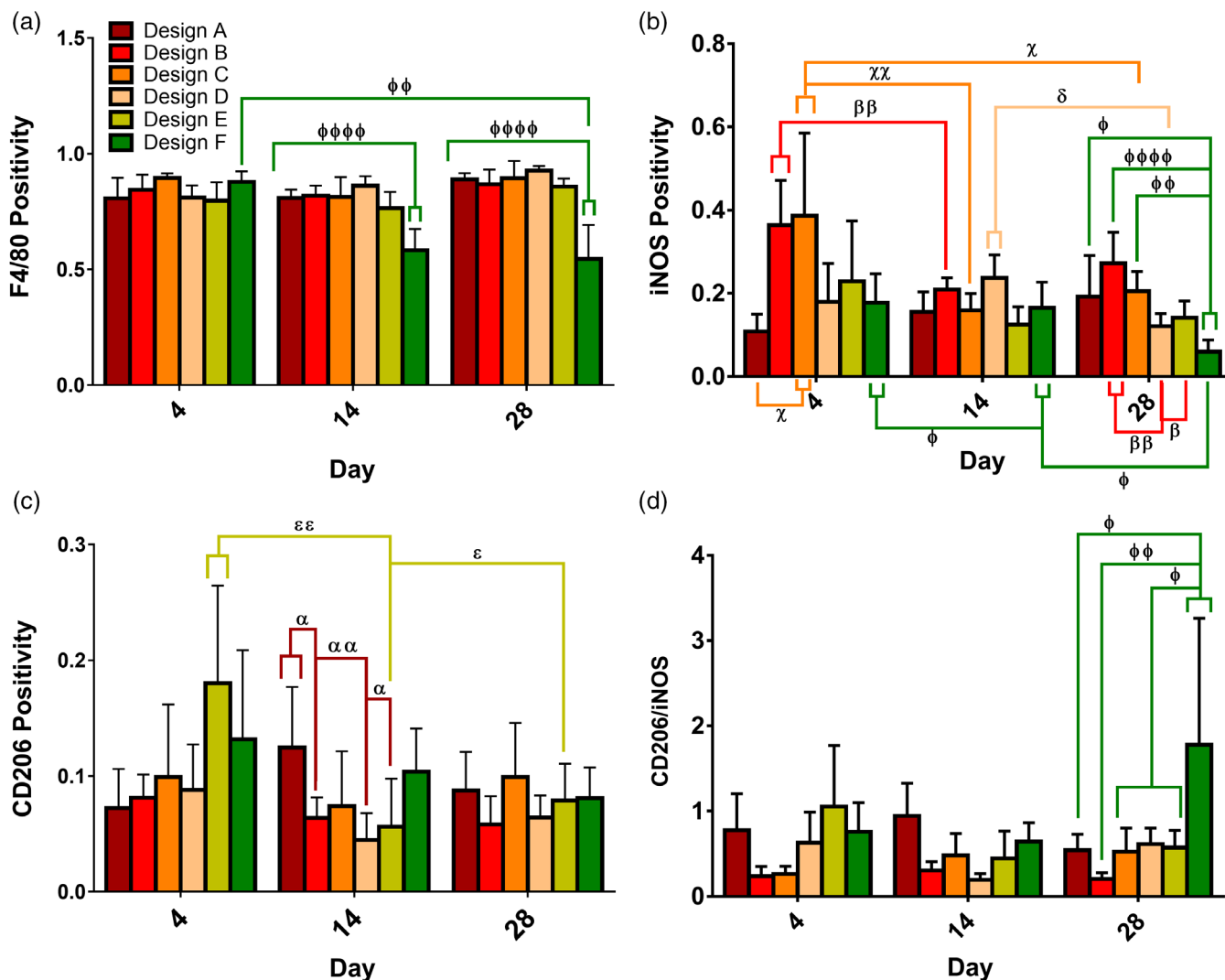


FIGURE 7 Macrophage phenotype characterization. Tissues were immunohistochemically stained to identify macrophage phenotype, with (a) F4/80 as a pan-macrophage marker, (b) iNOS as an M1 marker, and (c) CD206 as an M2 marker. (d) The CD206/iNOS ratio, representing the M2/M1 ratio, was also plotted. Greek symbols correspond to statistically significant differences detected between test group and the group with the same name in the English alphabet: $\alpha = p < .05$ between Design (a) and test, $\beta = p < .05$ from Design (b), $\gamma =$ diff. from (c), $\delta =$ diff from (d), $\epsilon =$ diff from (e), $\theta =$ diff. from (f). The color of each line indicating a significant difference matches that of the respective design

were analyzed via peptide-matching of LC-MS/MS data comparing macroporous designs (Designs a–d) and non/microporous controls (Designs e and f). Although none of the cross-matched comparisons were statistically significant between the macroporous and the non/microporous groups, there were some interesting top hits, defined as $p < .15$ and a $|\text{fold-change}| > 1.5$ (Table 3). Of the 3,172 proteins identified from LC-MS/MS at the polymer–tissue interface, a total of 10 proteins that were upregulated by macroporous SMP scaffolds, and 3 proteins that were downregulated, met these criteria. Upregulated proteins included those involved in wound healing (e.g., MMP-12) and protein translation and gene expression (e.g., phenylalanine-tRNA ligase beta subunit [SYFB] and MMP-12) (Consortium TU, 2018; Marchant et al., 2014). A protein involved in target of Rapamycin (TOR) signaling (e.g., Ras-related GTP-binding protein C [RRAGC]) (Proud, 2007), a nutrient, energy and redox regulator that

controls protein synthesis and cellular growth and migration (Proud, 2007), was also promoted. Proteins known to promote neutrophil chemotaxis, such as 55 kDa erythrocyte membrane protein (EM55) and interleukin-1 receptor antagonist protein (IL1RA) (Proud, 2007; Quinn et al., 2009), were also upregulated with macroporous SMP designs, which corroborates with inflammation score results that demonstrated more neutrophils were present with these designs. Similarly, lipoprotein lipase, shown elsewhere as a critical enzyme for triglyceride metabolism and in promoting macrophage-derived foam cell differentiation (Babaev, Patel, Semenkovich, Fazio, & Linton, 2000), was upregulated and coincides with a larger abundance of these cell types. Phagocytosis and endocytosis (e.g., MMP-12, phospholipase D4 [PLD4], FK506-binding protein 15 [FKB15], 26S proteasome non-ATPase regulatory subunit 5 (PSMD5)) also appear to be enhanced. Conversely, proteins downregulated by

TABLE 3 Top hits from proteomics analysis in terms of fold-change and closeness to significance

	Fold-change (p-value)	Protein	Gene	Protein ID	UniProtKB link	Biological function (Proud, 2007)
Upregulated by SMP macroporous scaffolds	3.92 (.1197)	Phenylalanine-tRNA ligase beta subunit	Farsb	Q9WUA2 (SYFB_MOUSE)	https://www.uniprot.org/uniprot/Q9WUA2	Protein heterotrimerization (part of cellular component biogenesis); phenylalanyl-tRNA aminoacylation, (part of protein translation and gene expression).
	3.08 (.0826)	Macrophage metalloelastase	Mmp12	P34960 (MMP12_MOUSE)	https://www.uniprot.org/uniprot/P34960	Possible role in tissue injury and remodeling; possesses significant elastolytic activity. Positive regulator of epithelial cell proliferation involved in wound healing, gene expression; interferon- α secretion, and proteolysis (Quinn et al., 2009).
	2.40 (.1273)	Eukaryotic translation initiation factor 2 subunit 3	Eif2s3x	Z9ZON1 (IF2G_MOUSE)	https://www.uniprot.org/uniprot/Z9ZON1	Early stages of protein synthesis; formation of translational preinitiation complex
	2.37 (.1377)	Lipoprotein lipase	Lpl	P11152 (LIPL_MOUSE)	https://www.uniprot.org/uniprot/P11152	Enzyme on lumen surface of vascular endothelium involved in triglyceride metabolism; plays key role in the clearance, utilization, and storage of lipids; positive regulator of macrophage-derived foam cell differentiation (Moritz et al., 1992).
	2.20 (.0768)	55 kDa erythrocyte membrane protein	Mpp1	P70290 (EM55_MOUSE)	https://www.uniprot.org/uniprot/P70290	Regulates neutrophil chemotaxis by regulating neutrophil polarity (Karayannacos et al., 1978).
	2.07 (.1009)	Ras-related GTP-binding protein C	Rragc	Q99K70 (RRAGC_MOUSE)	https://www.uniprot.org/uniprot/Q99K70	Binds GDP to form protein heterodimeric complexes that relocate mTORC1 to lysosomes, a critical step in activating TOR signaling cascade.
	1.85 (.0985)	Interleukin-1 receptor antagonist protein	Il1rn	P25085 (IL1RA_MOUSE)	https://www.uniprot.org/uniprot/P25085	Negative regulation of interleukin-1, apoptosis, cell migration, and membrane potential; involved in neutrophil chemotaxis.
	1.83 (.0604)	FK506-binding protein 15	Fkbp15	Q6P9Q6 (FKB15_MOUSE)	https://www.uniprot.org/uniprot/Q6P9Q6	Endocytosis; negative regulator of phosphatase activity; protein peptidyl-prolyl isomerization.
	1.80 (.1046)	Phospholipase D4	Plid4	Q8BG07 (PLD4_MOUSE)	https://www.uniprot.org/uniprot/Q8BG07	Phagocytosis; lipid catabolism.
	1.70 (.1347)	26S proteasome non-ATPase regulatory subunit 5	Psm5	Q8BJY1 (PSMD5_MOUSE)	https://www.uniprot.org/uniprot/Q8BJY1	Proteasome regulatory particle assembly, which is part of cellular component biogenesis.
Downregulated	-1.90 (.1285)	Calsequestrin-2	Casq2	O09161 (CASQ2_MOUSE)	https://www.uniprot.org/uniprot/O09161	Calcium-binding protein; plays important role in initiating muscle contraction.
	-1.80 (.0898)	60S ribosomal protein L39	Rpl39	P62892 (RL39_MOUSE)	https://www.uniprot.org/uniprot/P62892	Liver metabolism protein; antibacterial humoral response; cytoplasmic translation.
	-1.73 (.1092)	Gelsolin	Gsn	Q3SX14 (GELS_BOVIN)	https://www.uniprot.org/uniprot/Q3SX14	Actin filament severing; actin nucleation, barbed-end actin filament capping.

Abbreviation: SMP, shape memory polymer.

macroporous SMP Designs a–d relative to non/microporous controls e and f include those involved in muscle contraction (calsequestrin-2 [CASQ2]), antibacterial responses (608 ribosomal protein L39), and actin cytoskeletal organization (Gelsolin [Q3SX14]).

IHC staining of MMP-12, which had the second-highest fold-change in macroporous designs compared to non/microporous ones (3.08), and the fourth-lowest *p*-value ($p = .0826$), corroborated the proteomics data. Quantification of IHC staining for Designs c and e revealed an MMP-12% positivity of 12.6 ± 9.51 and 4.13 ± 3.21 , respectively, which was almost statistically significant ($p = .0610$, Figure S12). Also consistent with the proteomics data, which showed fold expression of other MMPs to either be slightly positive (0.22 for MMP-13, $p = .9064$), slightly negative (-0.16 for MMP-9, $p = .9459$), or moderately negative (-0.54 to -1.59 for MMP-2, -14, -3, and -8, $p = .2423$ – 0.7145), macroporous designs appeared to upregulate MMP-12 the most of all MMPs tested by IHC (Figures S13–S17). Granular, cytoplasmic staining for MMPs was observed in several cell types, but most notably colocalized with macrophages peripheral to the polymer–tissue interface (i.e., within approximately 100 μm of the implant) (Table S9). This implied that macrophages infiltrating the polymer–tissue interface produce MMPs.

4 | DISCUSSION

PCL-based SMPs with a melting temperature below body temperature offer utility in biomedical applications where shape recovery and/or moldability at body temperature are beneficial, such as in minimally invasive surgical devices and constructs (Boire et al., 2015). Another potential utility is as an external stent to mitigate NH in vein grafts and hemodialysis access sites. The main aim of this study was to maximize neovascularization via controlled pore size and spacing because adventitial angiogenesis promotion has been correlated with NH reduction in several studies evaluating external sheaths in large animal models (Angelini et al., 1996; Boire et al., 2016; George et al., 2001; Jeremy et al., 2007; Mehta et al., 1998), purportedly due to an outward rather than inward migratory shift of VSMCs (Jeremy et al., 2007). It is less clear what degree of inflammation and foreign body reaction is ideal for external stenting, but it has been shown that complement and mast cells migrate onto NH-reducing macroporous polyester (Dacron) sheaths and deposit ECM proteins; lymphocytes, neutrophils, and giant cells (George et al., 2001), but not with ineffective microporous ePTFE stents (Karayannacos et al., 1978; Moritz et al., 1992). Qualitatively, the macroporous SMP scaffolds promote a similar inflammatory and immune response.

Compared to ePTFE, a relatively inert, nondegradable polymer (Koehler et al., 2003), the noncytotoxic, slowly biodegradable, artery-mimetic, macroporous SMP designs paired by two equivalent pore sizes and spacings were pro-inflammatory, pro-neovascular, and profibrotic. Inflammation remained mild in all designs except for the closer-spaced, smaller-sized Design a, which was more moderate and had a significantly lower cumulative score than Design f as a result. The design most conducive to microvessel formation, the

wider-spaced, smaller pore Design c, had the highest M1 macrophage phenotype on Day 4 before significantly decreasing at later timepoints, corroborating previous findings that transient upregulation of an M1 macrophage phenotype can act as a pro-angiogenic stimulus (Yang et al., 2016). Pairwise comparisons of pore spacings and sizes on Day 28 indicated that smaller pores promoted more macrophages of a pro-tissue remodeling, pro-wound healing M2 phenotype, and that wider spacings downregulated the pro-inflammatory M1 macrophage phenotypes (Badylak, Valentin, Ravindra, McCabe, & Stewart-Akers, 2008). This implied that the $\sim 230 \mu\text{m}$ -spaced, $\sim 635 \mu\text{m}$ -sized Design c ultimately elicits an inflammatory response characterized by more of the “tissue remodeling” M2 phenotype than the other macroporous designs, which is thought to be desirable in the eventual resolving of tissue and in promoting a more sustained pro-angiogenic response (Spiller et al., 2014).

Some of the proteins identified from proteomics analysis as being upregulated from macroporous SMP scaffolds compared to non/microporous control implants coincided with histological observations. For example, proteins involved in neutrophil chemotaxis and macrophage-derived foam cell differentiation corroborated to some degree with the slightly lower inflammation scores of macroporous designs (Babaev et al., 2000; Proud, 2007; Quinn et al., 2009). A protein involved in TOR signaling (Proud, 2007), which is associated with protein synthesis and cell growth and migration (Proud, 2007), was also upregulated. MMP-12 upregulation was essentially confirmed through quantification of IHC stains against this protein, and this result provided partial validation of other proteins that were close-to-significantly upregulated or downregulated relative to non/microporous controls in the proteomics analysis. In the MMP-12 IHC, it appeared that MMP-12 colocalized with macrophages, consistent with other studies (Lindsey & Zamilpa, 2012), suggesting that MMP-12 is secreted from macrophages and may play a role in the neo-fibrovascular responses at the polymer–tissue interface. While its role in angiogenesis is complex—it has been shown to promote angiogenesis through release of pro-angiogenic factors and destruction of angiogenic inhibitors, as well as inhibit angiogenesis via upregulation of angiogenic inhibitors such as angiostatin or endostatin (Rundhaug, 2005; Stetler-Stevenson, 1999)—MMP-12 is posited to play an important role in tissue remodeling and wound healing (Consortium TU, 2018; Marchant et al., 2014), both in desirable and pathological ways (Lindsey & Zamilpa, 2012; Molet et al., 2005; Wells, Gaggari, & Blalock, 2015).

A key characteristic of MMP-12 is its strong elastolytic activity (Proud, 2007; Quinn et al., 2009), which is interesting as this is very similar to the purported mechanism by which Proteon Therapeutics' vonapanitase (PRT-201) functions. Vonapanitase is a 26-kDa recombinant human elastase delivered periaortally through a collagen gel that cleaves elastin fibers within blood vessel walls to induce outward remodeling of AVFs (Peden et al., 2017). Similar to external stent studies (Jeremy et al., 2007), it is purported that this can reduce NH by altering the migration of VSMCs toward the adventitia rather than the intima (Peden et al., 2017). Other therapeutic approaches developed but not FDA-approved in this space are pro-angiogenic and

function in a similar manner, including a replication-deficient adenoviral vector constitutively expressing VEGF-D (Ark Therapeutics' Trinam) (Fuster, Charlton, & Boyd, 2001) and an aortic endothelial cell treatment embedded in gelatin (Shire's VascuGel) (Conte et al., 2009). Vonapanitase demonstrated an increase in blood flow rates and outflow vein diameters of AVFs and AVGs in rabbit and porcine models (Burke, Franano, Mendenhall, et al., 2008; Burke, Franano, LaRochelle, & Mendenhall, 2008; Burke, Mendenhall, Larochelle, & Franano, 2009; Franano, Hance, Bland, & Burke, 2007). However, it failed to show a reduction in NH at 21 days in a 12-pig AVG study (Burke et al., 2009), and recently failed to achieve statistical significance on both of its coprimary endpoints in a second Phase III clinical trial (PATENCY-2) seeking to improve maturation and patency of AVFs. These results may underpin the importance of providing a more sustained effect with an external sheath, perhaps with a slowly biodegradable SMP wrap that promotes MMP-12 expression periaxially, rather than with a therapeutic that may exude only short-term effects (catalytic activity of 1–4 hr) (Wong et al., 2016). Further in-depth studies are required to confirm and elucidate the role that MMP-12 might play in the neovascular, inflammatory, and fibrogenic responses to these macroporous SMP scaffolds.

There are several limitations to this study, the most salient of which is the difference in tissue responses between the subcutaneous environment investigated here and the perivascular environment to which these SMP scaffolds are to be applied for AVF/AVG and PABG/CABG surgery applications. VSMCs, endothelial cells, and myofibroblasts abundant within and along the exterior of blood vessels all play critical roles in the remodeling processes of vascular tissues, and may be in lower abundance and/or behave differently in the subcutaneous environment. Moreover, perivascular adipose tissue has been shown to influence inflammation, vasoreactivity, and VSMC proliferation, and is distinct from subcutaneous adipose tissue (Rajshaker et al., 2010). The proximity of recirculating blood cells to the implant site in a periaxial setting will also alter inflammatory and immune responses. Nonetheless, all implants will undergo a wound healing process consisting of homeostasis, inflammation, repair, and remodeling, regardless of their tissue environment, and macrophages and other inflammatory cells present in both environments will play a central role in the tissue responses observed. It is for this reason that the principle findings of this study—namely, the effect of pore size and spacing on neovascularization, inflammation, and fibrogenesis—are anticipated to translate to a perivascular environment. Further studies are planned in both small and large animal vascular environments to more precisely evaluate the role that these processes play in NH. A more meaningful cumulative score metric can also be derived from such studies that properly weigh these three criteria in terms of their importance in perivascular applications.

Another limitation of this study is its relatively short duration of 28 days *in vivo*. Inflammatory responses will continue for many months and through the full resorption of the scaffold. Consistent with classic remodeling and wound healing processes, however, 30 days has been shown with other, biodegradable (polyurethane-based) SMPs to be an important transition phase where acute inflammatory reactions are still

active, but begin to give way to macrophage-directed remodeling to granulation tissue (Jessen et al., 2020). Indeed, it is generally known that key inflammatory and remodeling phases have peaked and/or are resolved by 3 weeks (Anderson, Rodriguez, & Chang, 2008; Li, Chen, & Kirsner, 2007). Therefore, while inflammation and connective tissue remodeling may continue to a degree beyond 1 month due to the persistence of the implant, it can be argued that the initial events captured in the 28-day timepoint have a significant and likely fate-determining impact on the ultimate outcome from the implant. The significant fibrovascular formation induced by the macroporous PCL-based SMPs at 28 days in this study, and the apparent role of macrophages and MMPs in the process, seem to be consistent with this classic type of tissue remodeling. Although longer term inflammatory responses have not yet been characterized with these scaffolds, Jessen et al. observed similar overall inflammatory scores at 30, 90, and 180 days with their polyurethane-based SMPs, as acute inflammation was phased out in favor of inflammatory responses related to tissue remodeling and wound healing. It is fair to expect a similar type of inflammatory response as the macroporous SMPs degrade, but further study is required. The findings described herein, along with additional studies characterizing perivascular responses at more extended timepoints, will be instrumental to improving perivascular wrap function and maturation and patency outcomes for hemodialysis, coronary bypass, and peripheral bypass patients.

5 | CONCLUSIONS

The role of pore size and spacing of SMP scaffolds on neovascularization, inflammation, and fibrogenic responses was evaluated *in vivo*. Slowly biodegradable, PCL-based SMP scaffolds significantly upregulated neovascularization and fibrogenesis relative to nonporous SMP and microporous ePTFE implants at 28 days, while inflammation remained mild. CD31 staining revealed that macroporous SMP scaffolds, and in particular wider-spaced Designs c and d, promoted neovascularization significantly more so than non/microporous controls. Fibrogenesis also appeared to be upregulated from macroporous SMPs, as assessed by the degree of connective tissue bridging of the implants after 28 days by H&E and Masson's trichrome staining. IHC-based macrophage phenotype characterization indicated that pro-inflammatory M1 macrophages identified from iNOS staining were significantly and transiently upregulated in macroporous SMP Design d (640 μm diameter, 223 μm spacing) relative to A (627 μm pore size, 148 μm spacing) at Day 4, which correlated with angiogenesis as previously reported. Combined with the observation that smaller pores promoted more macrophages of an M2 phenotype at 28 days, these results suggest that the 223 μm -spaced, 640 μm -sized Design c elicits an inflammatory response characterized by a desirable "wound healing" M2 phenotype relative to the other macroporous designs. While additional studies at more extensive timepoints in a perivascular environment are required to realize the implications of these results, findings from this study warrant further investigation of this perivascular SMP approach.

ACKNOWLEDGMENTS

This work was supported by a National Center for Advancing Translational Sciences (NCATS)/National Institute of Health (NIH) Vanderbilt Institute for Clinical and Translational Research (VICTR) Award (UL1 TR000445), NIH R01 HL122347, a National Science Foundation Grant (NSF AIR-TT 1542996), and an American Heart Association Predoctoral Fellowship (AHA 15PRE25610014). The Translational Pathology Shared Resource (TPSR) is supported by NCI/NIH Cancer Center Support Grant 5P30 CA68485-19 and the Vanderbilt Mouse Metabolic Phenotyping Center Grant 2 U24 DK059637-16.

Special thanks to the entire Vanderbilt Translational Pathology Shared Resource, in particular Dr Kelli Boyd, DVM, PhD, for her guidance, as well as the hard work of Frances Shook and Cindy Lowe, as this work would not have been possible without them. Special thanks also to Kristie Rose, PhD and Hayes McDonald, PhD, that ran LC-MS/MS on samples and conducted proteomics analysis using software within Vanderbilt University's MSRC Proteomics Core. Additional thanks to Joseph Roland, PhD, for his help in conducting the CD31 microvessel detection analysis using the Digital Image Hub hosted by the Digital Histology Shared Resource at VUMC. The authors would also like to acknowledge Mr Dan Ayers, MS; James C. Slaughter, DrPH; Tatsuki Koyama, PhD; and Frank E. Harrell, Jr., PhD in the Department of Biostatistics, VUMC, for assistance with statistical analysis and strategy via Vanderbilt's Biostatistics Clinic. Thanks to Brian O'Grady, PhD and Leon Bellan, PhD, for supplying human dermal fibroblasts and cell culture space for cytotoxicity testing. Thanks as well to Dr Hak-Joon Sung, Department of Biomedical Engineering, Vanderbilt University, for partial financial support of this work.

REFERENCES

- Abbott, W. M., Megerman, J., Hasson, J. E., L'Italien, G., & Warnock, D. F. (1987). Effect of compliance mismatch on vascular graft patency. *Journal of Vascular Surgery*, 5(2), 376–382.
- Alexander, J. H., Hafley, G., Harrington, R. A., Peterson, E. D., Ferguson, T. B., Jr., Lorenz, T. J., et al. (2005). Efficacy and safety of edifoligide, an E2F transcription factor decoy, for prevention of vein graft failure following coronary artery bypass graft surgery: PREVENT IV: A randomized controlled trial. *JAMA*, 294(19), 2446–2454.
- Al-Jaishi, A. A., Oliver, M. J., Thomas, S. M., Lok, C. E., Zhang, J. C., Garg, A. X., ... Moist, L. M. (2014). Patency rates of the arteriovenous fistula for hemodialysis: A systematic review and meta-analysis. *American Journal of Kidney Diseases*, 63(3), 464–478.
- Anderson, J. M., Rodriguez, A., & Chang, D. T. (2008). Foreign body reaction to biomaterials. *Seminars in Immunology*, 20(2), 86–100.
- Angelini, G. D., Izzat, M. B., Bryan, A. J., & Newby, A. C. (1996). External stenting reduces early medial and neointimal thickening in a pig model of arteriovenous bypass grafting. *The Journal of Thoracic and Cardiovascular Surgery*, 112(1), 79–84.
- Babaev, V. R., Patel, M. B., Semenkovich, C. F., Fazio, S., & Linton, M. F. (2000). Macrophage lipoprotein lipase promotes foam cell formation and atherosclerosis in low density lipoprotein receptor-deficient mice. *Journal of Biological Chemistry*, 275(34), 26293–26299.
- Badero, O. J., Salifu, M. O., Wasse, H., & Work, J. (2008). Frequency of swing-segment stenosis in referred dialysis patients with Angiographically documented lesions. *American Journal of Kidney Diseases*, 51(1), 93–98.
- Badylak, S. F., Valentin, J. E., Ravindra, A. K., McCabe, G. P., & Stewart-Akers, A. M. (2008). Macrophage phenotype as a determinant of biologic scaffold remodeling. *Tissue Engineering Part A*, 14(11), 1835–1842.
- Ballyk, P. D., Walsh, C., Butany, J., & Ojha, M. (1997). Compliance mismatch may promote graft-artery intimal hyperplasia by altering suture-line stresses. *Journal of Biomechanics*, 31(3), 229–237.
- Bankhead, P., Loughrey, M. B., Fernández, J. A., Dombrowski, Y., McArt, D. G., Dunne, P. D., et al. (2017). QuPath: Open source software for digital pathology image analysis. *Scientific Reports*, 7(1), 16878.
- Boire, T. C., Balikov, D. A., Lee, Y., Guth, C. M., Cheung-Flynn, J., & Sung, H.-J. (2016). Biomaterial-based approaches to address vein graft and hemodialysis access failures. *Macromolecular Rapid Communications*, 37(23), 1860–1880.
- Boire, T. C., Gupta, M. K., Zachman, A. L., Lee, S. H., Balikov, D. A., Kim, K., ... Sung, H.-J. (2015). Pendant allyl crosslinking as a tunable shape memory actuator for vascular applications. *Acta Biomaterialia*, 24, 53–63.
- Bourassa, M., Fisher, L., Campeau, L., Gillespie, M., McConney, M., & Lesperance, J. (1985). Long-term fate of bypass grafts: The coronary artery surgery study (CASS) and Montreal Heart Institute experiences. *Circulation*, 72(6 Pt 2), V71–V78.
- Brown, B. N., Londono, R., Tottey, S., Zhang, L., Kukla, K. A., Wolf, M. T., ... Badylak, S. F. (2012). Macrophage phenotype as a predictor of constructive remodeling following the implantation of biologically derived surgical mesh materials. *Acta Biomaterialia*, 8(3), 978–987.
- Bunt, T. (2001). Vascular graft infections: An update. *Cardiovascular Surgery*, 9(3), 225–233.
- Burke, S., Franano, F., LaRochelle, A., & Mendenhall, H. (2008). Local application of recombinant human type I pancreatic elastase (PRT-201) to an arteriovenous fistula (AVF) increases AVF blood flow in a rabbit model. *Journal of the American Society of Nephrology*, 19, 252–253A.
- Burke, S., Franano, F., Mendenhall, H., Howk, K., LaRochelle, A., & Wong, M. (2008). Recombinant human elastase (PRT-201) dilates outflow veins in a rabbit mode of arteriovenous fistula. *Journal of the American Society of Nephrology*, 18, 34A.
- Burke, S., Mendenhall, H., Larochele, A., & Franano, F. (2009). Recombinant human pancreatic elastase (prt-201) dilates the arteriovenous graft (AVG) outflow vein and increases graft blood flow in a porcine femoral AVG model. *The Journal of Vascular Access*, 10(2), 84.
- Carmeliet, P., & Jain, R. K. (2000). Angiogenesis in cancer and other diseases. *Nature*, 407(6801), 249–257.
- Chanakira, A., Dutta, R., Charboneau, R., Barke, R., Santilli, S. M., & Roy, S. (2012). Hypoxia differentially regulates arterial and venous smooth muscle cell proliferation via PDGFR- β and VEGFR-2 expression. *American Journal of Physiology - Heart and Circulatory Physiology*, 302(5), H1173–H1184.
- Chesebro, J. H., Fuster, V., Elveback, L. R., Clements, I. P., Smith, H. C., Holmes, D. R. J., et al. (1984). Effect of dipyridamole and aspirin on late vein-graft patency after coronary bypass operations. *New England Journal of Medicine*, 310(4), 209–214.
- Consortium TU. (2018). UniProt: A worldwide hub of protein knowledge. *Nucleic Acids Research*, 47(D1), D506–D515.
- Conte, M. S. (2007). Molecular engineering of vein bypass grafts. *Journal of Vascular Surgery*, 45(Suppl 6), A74–A81.
- Conte, M. S., Bandyk, D. F., Clowes, A. W., Moneta, G. L., Seely, L., Lorenz, T. J., et al. (2006). Results of PREVENT III: A multicenter, randomized trial of edifoligide for the prevention of vein graft failure in lower extremity bypass surgery. *Journal of Vascular Surgery*, 43(4), 742–751 discussion 751.
- Conte, M. S., Nugent, H. M., Gaccione, P., Guleria, I., Roy-Chaudhury, P., & Lawson, J. H. (2009). Multicenter phase I/II trial of the safety of allogeneic endothelial cell implants after the creation of arteriovenous access for hemodialysis use: The V-HEALTH study. *Journal of Vascular Surgery*, 50(6), 1359–1368.e1.

- Cox, J., Hein, M. Y., Lubner, C. A., Paron, I., Nagaraj, N., & Mann, M. (2014). Accurate proteome-wide label-free quantification by delayed normalization and maximal peptide ratio extraction, termed MaxLFQ. *Molecular and Cellular Proteomics: MCP*, 13(9), 2513–2526.
- Cunnane, C. V., Cunnane, E. M., & Walsh, M. T. (2017). A review of the hemodynamic factors believed to contribute to vascular access dysfunction. *Cardiovascular Engineering and Technology*, 8(3), 280–294.
- Deeken, C. R., Melman, L., Jenkins, E. D., Greco, S. C., Frisella, M. M., & Matthews, B. D. (2011). Histologic and biomechanical evaluation of crosslinked and non-crosslinked biologic meshes in a porcine model of ventral incisional hernia repair. *Journal of the American College of Surgeons*, 212(5), 880–888.
- Dixon, B. S., Beck, G. J., Vazquez, M. A., Greenberg, A., Delmez, J. A., Allon, M., et al. (2009). Effect of dipyridamole plus aspirin on hemodialysis graft patency. *New England Journal of Medicine*, 360(21), 2191–2201.
- Edwards, W. H., Martin, R. S., Jenkins, J. M., & Mulherin, J. L. (1987). Primary graft infections. *Journal of Vascular Surgery*, 6(3), 235–239.
- Evans, B. C., Hocking, K. M., Kilchrist, K. V., Wise, E. S., Brophy, C. M., & Duvall, C. L. (2015). Endosomolytic nano-polyplex platform technology for cytosolic peptide delivery to inhibit pathological vasoconstriction. *ACS Nano*, 9(6), 5893–5907.
- Evans, B. C., Hocking, K. M., Osgood, M. J., Voskresensky, I., Dmowska, J., Kilchrist, K. V., ... Duvall, C. L. (2015). MK2 inhibitory peptide delivered in nanopolyplexes prevents vascular graft intimal hyperplasia. *Science Translational Medicine*, 7(291), 291ra95–291ra95.
- Fitzgibbon, G. M., Kafka, H. P., Leach, A. J., Keon, W. J., Hooper, G. D., & Burton, J. R. (1996). Coronary bypass graft fate and patient outcome: Angiographic follow-up of 5,065 grafts related to survival and reoperation in 1,388 patients during 25 years. *Journal of the American College of Cardiology*, 28(3), 616–626.
- Franano, F. N., Hance, K., Bland, K., & Burke, S. (2007). *PRT-201 dilates outflow veins and improves maturation rates in a rabbit model of AVF* (pp. 155–156). Oxford, England: Oxford University Press.
- Fuster, V., Charlton, P., & Boyd, A. (2001). Clinical protocol. A phase IIb, randomized, multicenter, double-blind study of the efficacy and safety of Trinam (EG004) in stenosis prevention at the graft-vein anastomosis site in dialysis patients. *Human Gene Therapy*, 12(16), 2025–2027.
- George, S. J., Izzat, M. B., Gadsdon, P., Johnson, J. L., Yim, A. P. C., Wan, S., ... Jeremy, J. Y. (2001). Macro-porosity is necessary for the reduction of neointimal and medial thickening by external stenting of porcine saphenous vein bypass grafts. *Atherosclerosis*, 155(2), 329–336.
- Goldman, S., Copeland, J., Moritz, T., Henderson, W., Zadina, K., Ovitt, T., ... Khuri, S. (1994). Long-term graft patency (3 years) after coronary artery surgery. Effects of aspirin: Results of a VA cooperative study. *Circulation*, 89(3), 1138–1143.
- Greca, F. H., Souza-Filho, Z. A., Giovanini, A., Rubin, M. R., Kuenzer, R. F., Reese, F. B., & Araujo, L. M. (2008). The influence of porosity on the integration histology of two polypropylene meshes for the treatment of abdominal wall defects in dogs. *Hernia*, 12(1), 45–49.
- Haruguchi, H., & Teraoka, S. (2003). Intimal hyperplasia and hemodynamic factors in arterial bypass and arteriovenous grafts: A review. *Journal of Artificial Organs*, 6(4), 227–235.
- Huber, T. S., Carter, J. W., Carter, R. L., & Seeger, J. M. (2003). Patency of autogenous and polytetrafluoroethylene upper extremity arteriovenous hemodialysis accesses: A systematic review. *Journal of Vascular Surgery*, 38(5), 1005–1011.
- Hye, R. J., Peden, E. K., O'Connor, T. P., Browne, B. J., Dixon, B. S., Schanzer, A. S., ... Burke, S. K. (2014). Human type I pancreatic elastase treatment of arteriovenous fistulas in patients with chronic kidney disease. *Journal of Vascular Surgery*, 60(2), 454–461.e1.
- Jeremy, J. Y., Bulbulia, R., Johnson, J. L., Gadsdon, P., Vijayan, V., Shukla, N., ... Angelini, G. D. (2004). A bioabsorbable (polyglactin), non-restrictive, external sheath inhibits porcine saphenous vein graft thickening. *The Journal of Thoracic and Cardiovascular Surgery*, 127(6), 1766–1772.
- Jeremy, J. Y., Gadsdon, P., Shukla, N., Vijayan, V., Wyatt, M., Newby, A. C., & Angelini, G. D. (2007). On the biology of saphenous vein grafts fitted with external synthetic sheaths and stents. *Biomaterials*, 28(6), 895–908.
- Jessen, S. L., Friedemann, M. C., Mullen, A. E., Ginn-Hedman, A.-M., Herting, S. M., Maitland, D. J., & Clubb, F. J., Jr. (2020). Micro-CT and histopathology methods to assess host response of aneurysms treated with shape memory polymer foam-coated coils versus bare metal coil occlusion devices. *Journal of Biomedical Materials Research Part B: Applied Biomaterials*, 108(5), 2238–2249.
- Karageorgiou, V., & Kaplan, D. (2005). Porosity of 3D biomaterial scaffolds and osteogenesis. *Biomaterials*, 26(27), 5474–5491.
- Karayannacos, P. E., Hostetler, J. R., Bond, M. G., Kakos, G. S., Williams, R. A., Kilman, J. W., & Vasko, J. S. (1978). Late failure in vein grafts: Mediating factors in subendothelial fibromuscular hyperplasia. *Annals of Surgery*, 187(2), 183–188.
- Karimi, A., Navidbakhsh, M., Shojaei, A., & Faghihi, S. (2013). Measurement of the uniaxial mechanical properties of healthy and atherosclerotic human coronary arteries. *Materials Science and Engineering: C*, 33(5), 2550–2554.
- Kim, B. J., Lim, J. W., Park, J. H., & Lee, Y. H. (2014). Dual plane augmentation genioplasty using Gore-Tex chin implants. *Archives of Craniofacial Surgery*, 15(2), 82–88.
- Klinge, U., & Klosterhalfen, B. (2012). Modified classification of surgical meshes for hernia repair based on the analyses of 1,000 explanted meshes. *Hernia*, 16(3), 251–258.
- Klosterhalfen, B., & Klinge, U. (2013). Retrieval study at 623 human mesh explants made of polypropylene—Impact of mesh class and indication for mesh removal on tissue reaction. *Journal of Biomedical Materials Research Part B: Applied Biomaterials*, 101(8), 1393–1399.
- Koehler, R. H., Begos, D., Berger, D., Carey, S., LeBlanc, K., Park, A., ... Voeller, G. (2003). Minimal adhesions to ePTFE mesh after laparoscopic ventral incisional hernia repair: Reoperative findings in 65 cases. *Zentralblatt für Chirurgie*, 128(08), 625–630.
- Kuchariková, S., Vande Velde, G., Himmelreich, U., & van Dijk, P. (2015). *Candida albicans* biofilm development on medically-relevant foreign bodies in a mouse subcutaneous model followed by bioluminescence imaging. *JoVE*, 95, e52239.
- Lake, S. P., Ray, S., Zihni, A. M., Thompson, D. M., Jr., Gluckstein, J., & Deeken, C. R. (2015). Pore size and pore shape—But not mesh density—Alter the mechanical strength of tissue ingrowth and host tissue response to synthetic mesh materials in a porcine model of ventral hernia repair. *Journal of the Mechanical Behavior of Biomedical Materials*, 42, 186–197.
- Li, J., Chen, J., & Kirsner, R. (2007). Pathophysiology of acute wound healing. *Clinics in Dermatology*, 25(1), 9–18.
- Li, L., Terry, C. M., Shiu, Y.-T. E., & Cheung, A. K. (2008). Neointimal hyperplasia associated with synthetic hemodialysis grafts. *Kidney International*, 74(10), 1247–1261.
- Lindsey, M. L., & Zamilpa, R. (2012). Temporal and spatial expression of matrix metalloproteinases and tissue inhibitors of metalloproteinases following myocardial infarction. *Cardiovascular Therapeutics*, 30(1), 31–41.
- Lok, C. E., Sontrop, J. M., Tomlinson, G., Rajan, D., Cattral, M., Oreopoulos, G., ... Moist, L. (2013). Cumulative patency of contemporary fistulas versus grafts (2000–2010). *Clinical Journal of the American Society of Nephrology*, 8(5), 810–818.
- MacRae, J. M., Dipchand, C., Oliver, M., Moist, L., Lok, C., Clark, E., et al. (2016). Arteriovenous access failure, stenosis, and thrombosis. *Canadian Journal of Kidney Health and Disease*, 3, 2054358116669126–2054358116669126.
- Marchant, D. J., Bellac, C. L., Moraes, T. J., Wadsworth, S. J., Dufour, A., Butler, G. S., et al. (2014). A new transcriptional role for matrix metalloproteinase-12 in antiviral immunity. *Nature Medicine*, 20, 493–502.

- Maurus, P. B., & Kaeding, C. C. (2004). Bioabsorbable implant material review. *Operative Techniques in Sports Medicine*, 12(3), 158–160.
- McGeachie, J., Meagher, S., & Prendergast, F. (1989). Vein-to-artery grafts: The long-term development of neo-intimal hyperplasia and its relationship to vasa vasorum and sympathetic innervation. *Australian and New Zealand Journal of Surgery*, 59(1), 59–65.
- Mehta, D., George, S. J., Jeremy, J. Y., Izzat, M. B., Southgate, K. M., Bryan, A. J., ... Angelini, G. D. (1998). External stenting reduces long-term medial and neointimal thickening and platelet derived growth factor expression in a pig model of arteriovenous bypass grafting. *Nature Medicine*, 4(2), 235–239.
- Misra, S., Fu, A. A., Misra, K. D., Shergill, U. M., Leof, E. B., & Mukhopadhyay, D. (2010). Hypoxia induces a phenotypic switch of fibroblasts to myofibroblasts through a MMP-2/TIMP mediated pathway: Implications for venous neointimal hyperplasia in hemodialysis access. *Journal of Vascular and Interventional Radiology: JVIR*, 21(6), 896–902.
- Molet, S., Belleguic, C., Lena, H., Germain, N., Bertrand, C. P., Shapiro, S. D., ... Lagente, V. (2005). Increase in macrophage elastase (MMP-12) in lungs from patients with chronic obstructive pulmonary disease. *Inflammation Research: Official Journal of the European Histamine Research Society*, 54(1), 31–36.
- Moritz, A., Grabenwöger, F., Raderer, F., Ptakovsky, H., Staudacher, M., Magometschnigg, H., ... Wolner, E. (1992). Mesh tube—Constricted varicose veins used as bypass grafts for infrainguinal arterial reconstruction. *Archives of Surgery*, 127(4), 416–420.
- Muto, A., Model, L., Ziegler, K., Eghbali, S. D., & Dardik, A. (2010). Mechanisms of vein graft adaptation to the arterial circulation: Insights into the neointimal algorithm and management strategies. *Circulation Journal: Official Journal of the Japanese Circulation Society*, 74(8), 1501–1512.
- Okuhn, S. P., Connelly, D. P., Calakos, N., Ferrell, L., Man-Xiang, P., & Goldstone, J. (1989). Does compliance mismatch alone cause neointimal hyperplasia? *Journal of Vascular Surgery*, 9, 35–45.
- Pappano, A. J., & Gil Wier, W. (2013). The microcirculation and lymphatics. In A. J. Pappano & W. Gil Wier (Eds.), *Cardiovascular physiology* (10th ed., pp. 153–170). Philadelphia, PA: Content Repository Only.
- Peden, E. K., O'Connor, T. P., Browne, B. J., Dixon, B. S., Schanzer, A. S., Jensik, S. C., ... Burke, S. K. (2017). Arteriovenous fistula patency in the 3 years following vonapanitase and placebo treatment. *Journal of Vascular Surgery*, 65(4), 1113–1120.
- Proud, C. G. (2007). Amino acids and mTOR signalling in anabolic function. *Biochemical Society Transactions*, 35(5), 1187–1190.
- Quinn, B. J., Welch, E. J., Kim, A. C., Lokuta, M. A., Huttenlocher, A., Khan, A. A., ... Chishti, A. H. (2009). Erythrocyte scaffolding protein p55/MPP1 functions as an essential regulator of neutrophil polarity. *Proceedings of the National Academy of Sciences of the United States of America*, 106(47), 19842–19847.
- Rajshaker, S., Manka, D., Blomkalns, A. L., Chatterjee, T. K., Stoll, L. L., & Weintraub, N. L. (2010). Crosstalk between perivascular adipose tissue and blood vessels. *Current Opinion in Pharmacology*, 10(2), 191–196.
- Roosa, S. M. M., Kemppainen, J. M., Moffitt, E. N., Krebsbach, P. H., & Hollister, S. J. (2010). The pore size of polycaprolactone scaffolds has limited influence on bone regeneration in an in vivo model. *Journal of Biomedical Materials Research Part A*, 92A(1), 359–368.
- Roy-Chaudhury, P., Sukhatme, V. P., & Cheung, A. K. (2006). Hemodialysis vascular access dysfunction: A cellular and molecular viewpoint. *Journal of the American Society of Nephrology*, 17(4), 1112–1127.
- Rundhaug, J. E. (2005). Matrix metalloproteinases and angiogenesis. *Journal of Cellular and Molecular Medicine*, 9(2), 267–285.
- Sabik Iii, J. F., Lytle, B. W., Blackstone, E. H., Houghtaling, P. L., & Cosgrove, D. M. (2005). Comparison of saphenous vein and internal thoracic artery graft patency by coronary system. *The Annals of Thoracic Surgery*, 79(2), 544–551.
- Sabik, J. F. (2011). Understanding saphenous vein graft patency. *Circulation*, 124(3), 273–275.
- Sivanesan, S., How, T. V., & Bakran, A. (1999). Sites of stenosis in AV fistulae for haemodialysis access. *Nephrology Dialysis Transplantation*, 14(1), 118–120.
- Spiller, K. L., Anfang, R., Spiller, K. J., Ng, J., Nakazawa, K. R., Daulton, J. W., & Vunjak-Novakovic, G. (2014). The role of macrophage phenotype in vascularization of tissue engineering scaffolds. *Biomaterials*, 35(15), 4477–4488.
- Stetler-Stevenson, W. G. (1999). Matrix metalloproteinases in angiogenesis: A moving target for therapeutic intervention. *The Journal of Clinical Investigation*, 103(9), 1237–1241.
- Stewart, S. F. C., & Lyman, D. J. (1992). Effects of a vascular graft/natural artery compliance mismatch on pulsatile flow. *Journal of Biomechanics*, 25, 297–310.
- System USRD. (2018). *2018 USRDS annual data report: Epidemiology of kidney disease in the United States*. Bethesda, MD: National Institutes of Health, National Institute of Diabetes and Digestive and Kidney Diseases.
- Trubel, W., Schima, H., Moritz, A., Raderer, F., Windisch, A., Ullrich, R., ... Polterauer, P. (1995). Compliance mismatch and formation of distal anastomotic intimal hyperplasia in externally stiffened and lumen-adapted venous grafts. *European Journal of Vascular and Endovascular Surgery*, 10(4), 415–423.
- Vijayan, V., Shukla, N., Johnson, J. L., Gadsdon, P., Angelini, G. D., Smith, F. C. T., ... Jeremy, J. Y. (2004). Long-term reduction of medial and intimal thickening in porcine saphenous vein grafts with a polyglactin biodegradable external sheath. *Journal of Vascular Surgery*, 40, 1011–1019.
- Wells, J. M., Gaggari, A., & Blalock, J. E. (2015). MMP generated matrikines. *Matrix Biology*, 44–46, 122–129.
- Wetmore, J. B., & Collins, A. J. (2016). Global challenges posed by the growth of end-stage renal disease. *Renal Replacement Therapy*, 2(1), 15.
- Wong, M. D., Bingham, K., Moss, E., Warn, J. D., Smirnov, I., Bland, K. S., ... Burke, S. K. (2016). Recombinant human elastase treatment of cephalic veins. *Cardiovascular Pharmacology: Open Access*, 5(2), 178.
- Yang, Y., Liu, F., Tang, M., Yuan, M., Hu, A., Zhan, Z., ... Lu, L. (2016). Macrophage polarization in experimental and clinical choroidal neovascularization. *Scientific Reports*, 6, 30933.
- Zhang, Z., Wang, Z., Liu, S., & Kodama, M. (2004). Pore size, tissue ingrowth, and endothelialization of small-diameter microporous polyurethane vascular prostheses. *Biomaterials*, 25(1), 177–187.
- Zhu, L.-M., Schuster, P., & Klinge, U. (2015). Mesh implants: An overview of crucial mesh parameters. *World Journal of Gastrointestinal Surgery*, 7(10), 226–236.

SUPPORTING INFORMATION

Additional supporting information may be found online in the Supporting Information section at the end of this article.

How to cite this article: Boire TC, Himmel LE, Yu F, et al.

Effect of pore size and spacing on neovascularization of a biodegradable shape memory polymer perivascular wrap.

J Biomed Mater Res. 2020;1–17. <https://doi.org/10.1002/jbm.a.37021>